FABRICATION OF NIOBIUM SHEET FOR RF CAVITIES

A Thesis

by

SHREYAS BALACHANDRAN

Submitted to the Office of Graduate Studies of
Texas A&M University
in partial fulfillment of the requirements for the degree of

MASTER OF SCIENCE

December 2008

Major Subject: Mechanical Engineering

FABRICATION OF NIOBIUM SHEET FOR RF CAVITIES

A Thesis

by

SHREYAS BALACHANDRAN

Submitted to the Office of Graduate Studies of
Texas A&M University
in partial fulfillment of the requirements for the degree of

MASTER OF SCIENCE

Approved by:

Chair of Committee, Richard. B. Griffin
Committee Members, Karl. T. Hartwig
Thomas. C. Pollock
Head of Department, Dennis O'Neal

December 2008

Major Subject: Mechanical Engineering

ABSTRACT

Fabrication of Niobium Sheet for RF Cavities.

(December 2008)

Shreyas Balachandran, B.E., RV College of Engineering, Bangalore

Chair of Advisory Committee: Dr. Richard B. Griffin

This thesis investigated the microstructure and mechanical property of RRR(high purity) and RG (low purity) niobium (Nb) sheet material. RRR Nb is used in the fabrication RF cavities. Our method involves processing bulk niobium by equal channel angular extrusion (ECAE) and then cross rolling to obtain sheets. This work is a study of the effect different thermomechanical processing variables have on the microstructure niobium sheets.

Recrystallization behaviors strongly depended on the purity levels. Tensile tests on sheets clearly indicated the anisotropy in the sheet material. The ductility of the sheet was found to be the largest at an angle of 45^{o} to the rolling direction. There was no apparent relationship observed in the yielding behavior in the different samples. The formability of the sheet measured by the anisotropy ratio suggested a strong dependence of anisotropy on texture. Texture results obtained show that different routes of ECAE can lead to variety of textures in final sheet material.

Correlations between the microstructure and the ECAE routes suggest that effective control of microstructure is possible by the thermomechanical steps followed in this study.

DEDICATION

I dedicate this thesis to my parents.

ACKNOWLEDGEMENTS

I would like to thank my committee chair, Dr. Griffin and my committee members Dr. Hartwig, and Dr. Pollock for their guidance and support throughout the course of this research. I have learned a lot from them, especially about the science and art of doing experiments. I would like to acknowledge Dr. Longnecker from the Statistics Department who willingly helped us with the generation of our test plan.

A special thanks goes to Robert from whom I have benefited through several useful discussions on a variety of topics, and Doug without whose support this work would have not been possible. I thank Dr.Karaman for letting me use their MTS machine for tensile tests. Can and Ji, thanks for bearing with me when I was using the machine. I thank my lab mate and friend, David, who has always been there ready to help, "Thank you sir". Of course, we shall sip on more coffee…

I thank all my friends from the materials group: Burak, Majid, Mohammed, Steven and Dan.

I would extend my gratitude towards the funding agency The Department of Energy, SBIR Program, whose financial support enabled me to be a research assistant throughout the course of my Masters studies.

Finally I would like to acknowledge the staff members of The Department of Mechanical Engineering who have always been available when I needed them.

All this would have not been possible if not for my wonderful parents who have always supported me in everything that I ever wanted to do.

TABLE OF CONTENTS

CHAPTER Page

LIST OF FIGURES

Page

Page

Page

Page

LIST OF TABLES

CHAPTER I

INTRODUCTION

Many applications desire microstructures that are homogeneous. Microstructural homogeneity takes into account grain size, texture and other microscopic components such as defect structures, sub grains etc. Microstructure – property – processing application relationships form the basis of materials engineering.

. The main aim of this work is to obtain homogeneous favorable microstructures in Nb sheets for a particular application of deep drawing. Favorable microstructures of sheet for forming applications refers to particular combinations of grain size usually less than 20 microns, and texture that will give the best properties for an application such as deep drawing. One particular texture that is favorable for deep drawing of bcc metals as reported in the literature seems to be the [111] crystallographic orientation normal to the plane of the sheet [1].

Any forming operation introduces directionality in the processed material, and one important factor in sheet metal forming is anisotropy, along with grain size. Anisotropy leads to non-uniform deformations in different directions. Anisotropy that exists in the plane of the sheet is called planar anisotropy and that which exists across the thickness is called normal or plastic anisotropy. Large grain sizes lead to an effect called orange peeling which is observed in the form of surface roughness when the sheet is stretched beyond the elastic limit [2].Normal anisotropy (R) is defined as the ratio of the plastic strain along the width to that along the thickness as shown in Figure 1.

This thesis follows the style and format of Mater.Sci.Eng. A

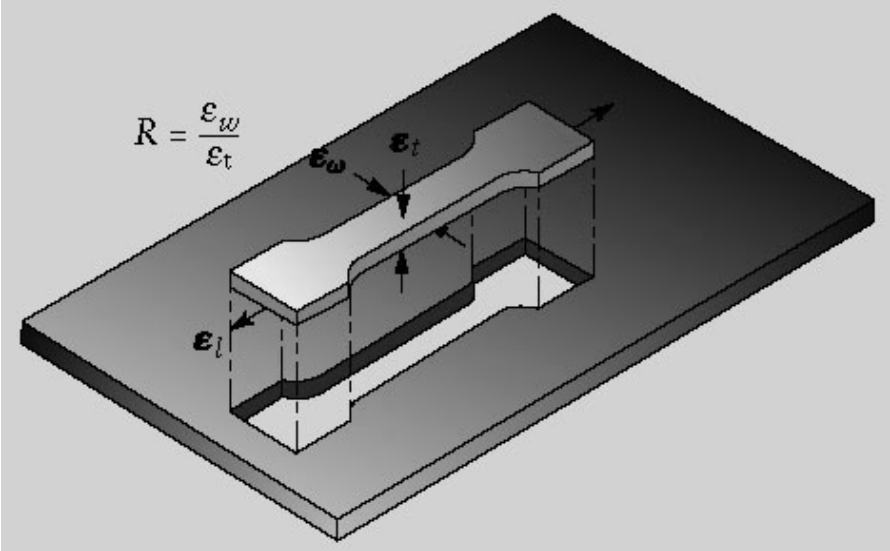

Figure 1. A schematic indicating the meaning of normal anisotropy(R) as the ratio of strains along the width to the thickness in a tensile specimen [2].

Mathematically R is described by equation (1) [2]

$$R = \frac{\ln(\frac{w_o}{w_f})}{\ln(\frac{t_o}{t_f})} \quad \text{.....(1)}$$

Since rolled sheets have planar anisotropy, the R value in different directions to the rolling direction will be different. A common procedure to represent the R value is in terms of the average R value in 0^o, 45^o and 90^o orientations from the rolling direction [2] given by equation (2).

$$\bar{R} = \frac{R_o + 2R_{45} + R_{90}}{4} \quad \text{.....(2)}$$

Another term that defines the planar anisotropy is given the difference of the average R value in the 0^o and 90^o directions to that in the 45^o direction to the rolling axis [2].

$$\Delta R = \frac{R_o - 2R_{45} + R_{90}}{2} \quad \text{.....(3)}$$

The variation in the R value shows up during the deep drawing operation in the form of the problem called earring. Figure 2 shows the earring observed in copper cups with different R value trends. It is clear that the most desirable characteristic of sheets is a high average R and a low ΔR.

There are some favorable textures that lead to such situations and such textures are known as balanced textures. These textures have a high fraction of [111] components also called the gamma fiber component and lower levels of [100] components also called the rotated cube components [3].

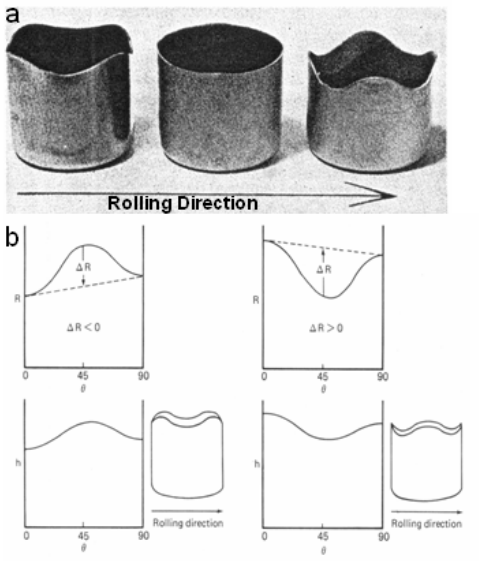

Figure 2. a. Copper cans that show earring behavior. The one on the left is the can with ΔR>0 and the one on the right is a can with ΔR<0. The can in the middle is the can with ΔR~0 which refers to the balance texture. b. Variation in the average R value in terms of the orientation and variation in the cup height with the orientation of the sheet [3].

The textures that develop in rolled sheets are directly related to the material crystallography and thermomechanical processing(TMP) conditions, prior strain history and heat treatments given [4].

The motivation of the present work is to control sheet texture by changing TMP conditions in order to arrive at favorable sheet microstructures. Conventional forming processes to break down the initial cast structures such as forging, extrusion and rolling do not easily breakdown the structure uniformly which may affect the material behavior in later fabrication steps. In order to exercise control over the fabrication processes it may be desired to have a uniform microstructure.

The approach that we have followed in this research is to process bulk Nb through a severe plastic deformation process called equal channel angular extrusion (ECAE).ECAE is an effective way to obtain a uniform deformation and hence uniform microstructure[5]. Textural control is also possible depending on the choice of route [6]. Nb processed via ECAE was subjected to different thermo mechanical histories, and then cross rolled and later annealed with the intent of obtaining sheets with lesser anisotropy and favorable textures as compared to commercially available sheet

This report presents results on the development of texture and microstructural anisotropy coming from the different variables involved in the processing.

CHAPTER II

LITERATURE SURVEY

A. Niobium-History, Properties and Applications

In the middle of 17th century along the banks of the river Columbia a mineral with golden streaks was discovered. In 1801, Charles Hatchett analyzed this mineral and identified a new element and called it Columbium. For a longtime this element was confused with its chemical twin Tantalum (Ta) as they always occur together and their chemical properties are so very similar. In 1844 Heinrich Rose, a German chemist clarified the situation by unequivocally showing the difference between the two elements and gave columbium a new name by which it is now recognized - niobium (Nb) [7].

Niobium is a body centered cubic (bcc) metal, which has a high melting point, good electrical and thermal conductivity and is highly formable at room temperature. Pure Nb can undergo up to 90% area reduction at room temperature before any intermediate heat treatment. Table 1 illustrates the properties of commercially pure wrought Nb.

Niobium deposits are extensively found in Brazil which is one of the chief producers of niobium ore as well as pure Nb [9]. The major consumption of Nb is in the form of ferroniobium a major component of a number of superalloyed steels. This application stems from the fact that Nb is a strong carbide former, stabilizes the carbon content in steels and by a combination of thermo mechanical processing the properties of steel can be engineered depending on the application [10]. Niobium and

Table 1. Summary of properties of wrought niobium[8]

Physical Properties	
Density	8.60 g/cc
Atomic Weight	92.906 g/mol
Crystal Lattice	b.c.c
Electrical Properties	
Electrical Resistivity (293K)	1.51×10^{-7} ohm.m
Thermal properties	
Coefficient of Linear Expansion (293 K)	7.10×10^{-6} /K
Thermal Conductivity (293 K)	52.3 W/m. K
Melting Point	2468 °C

its oxide powders are now being used as a capacitor material somewhat replacing tantalum in some applications[11].

Pure Nb and Nb alloys and compounds show Type II superconducting behavior. This superconducting property makes Nb a technologically important raw material for a variety of superconducting applications. Niobium- titanium alloys and niobium- tin compounds are extensively used in superconducting magnet applications. Pure Nb is widely used as superconducting pathway in rf cavities in particle accelerators, an application that will be dealt with in detail in the coming section. Table 2 lists some Nb products along with their application.

Table 2. Property application relationship between Niobium products [11].

Niobium Product	**Property**	**Application**
Ferro-niobium	Imparts strength, toughness	HSLA steels for oil and gas pipelines, car and truck bodies, ship hulls.
Niobium Oxide	High refractive index and transmittance, high dielectric constant	Coatings, Camera lenses, Ceramic capacitors
Niobium Carbide	High hardness, grain growth inhibitor	In cutting tools
Niobium Powder	High Dielectric constant, Formation of stable oxide dielectric	Capacitors
Niobium sheet, tubing, wires, rod and plates	Corrosion resistance, high temperature resistance, improved creep resistance, superconducting at 9.2K	Sputtering targets, cathode protection, chemical processing vessels, particle accelerator
Niobium Titanium, Niobium Tin	Superconducting at liquid He temperature(~4K)	Superconducting magnets in MRI's, particle physics experiments.
Niobium-1%Zirconium alloy	Corrosion resistance, fixation of oxygen	Chemical processing equipment

B. Conventional Forming of Niobium

The purity of Niobium is a major concern for many applications. Although the major impurity is usually Ta, it does not have a detrimental effect on most applications. However small changes in the concentrations of interstitials such as H, C, N,O can have a detrimental effect on the mechanical and electrical properties[12,13].

Extremely high purity Nb(>99.99%) is termed as RRR Niobium. RRR stands for Residual Resistivity Ratio, which is the ratio of the electrical resistance at ambient conditions to that at liquid helium temperatures in the non-superconducting state. A lower

purity Nb(~99.9%) is called RG (Reactor Grade). From here on we use the terminology RG and RRR to differentiate between the purity levels.

The exact details of producing of Nb with RRR > 300 depends on the company that manufacturers it [12,14,15]. Refining the material from commercial purity levels to high purity levels is done using a powder metallurgical process or melt metallurgical processes. In the powder metallurgical process the powder is pressed and sintered at round 2000C under high vacuum conditions. Sintering evaporates interstitial compounds and low melting impurities thus purifying the Nb. In the melt metallurgical process the ingot is fed into an electron beam (EB) furnace and remelted five or six times to remove the interstitial impurities. The Nb produced by this procedure is of extremely high purity and has RRR values greater than 300[15-16]. Though the same procedure is followed no two ingot slices have the same microstructure, industry considers this to be the statistical nature of the production[15]. Figure 3 shows a crossectional view of two billet slabs manufactured with the same processing parameters.

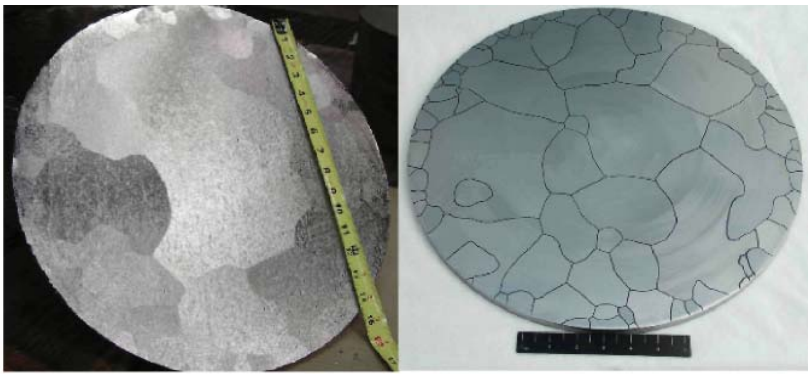

Figure 3. Large grained RRR niobium slices that came from a 430mm diameter ingots and were melted at the same melt rate, power and vacuum levels [15].

Forming operations can be classified broadly into primary and secondary working. Primary working processes generally refers breaking down a as cast billet into different shapes such as slabs, plates and billets. Typical primary working operations are: rolling, forging and extrusion. Secondary working deals with fabrication of shapes into final or semifinal components from a primary worked stage.

Another convenient way of classifying the deformation processes is according to the ratio of the surface area to the thickness deformed. A deformation where the surface area to the thickness ratio is low is termed bulk deformation and in the case of high surface area to thickness ratio it is termed sheet forming.[2]

As cast or EB melted Nb undergoes a series of forging, extrusion and rolling operations depending upon the final component that is desired. Details of the common manufacturing techniques used for RRR Nb can be found in references [14-16]. As our main focus is sheet material, we focus on the rolling operation and the sheet characteristics obtained by rolling.

1. Rolling

Our focus is on cold rolling, which refers to rolling done at room temperatures. The main parameters that are involved in rolling and the mechanics involved can be found in [2,17].

Rolling of sheets introduces anisotropy in the material, due to the development of textures in the rolled samples. Textures in any rolling operation are not only depend on the crystal lattice of the structure but also depend on the parameters of rolling [18]. The main parameters that affect the sheet texture are: a. Length of the sample in contact (L) to

the roll diameter ratio (d) commonly referred to as the L/d ratio. b. Percent reduction per pass. and c. Friction during rolling.

Rolled and fully annealed sheets usually have an elongated grain structure in the rolling direction which is a characteristic feature of a directional operation Our main focus is the texture evolution in rolled and annealed sheets and effects of the on the formability of sheets.

Niobium has a bcc crystal lattice and it is found that generally bcc rolled metals after annealing show a texture that is termed as fiber texture when viewed along the normal to the rolling direction. The main components of these textures are named the rotated cube[100] components, gamma fiber [111] components and [112] alpha fiber components [18].These are pictorially depicted in the form of orientation distribution functions (ODF's). Table 3 gives the components and Euler angles associated with annealed textures in bcc rolled sheets. Figure 4 shows a schematic ODF for a bcc metals.

Table 3. Ideal texture components of rolled and annealed bcc metals [19].

Component	$\{hkl\}\langle uvw\rangle$	Code[b]	Euler angles: Roe ψ, θ, ϕ / Matthies α, β, γ			Bunge[a] $\varphi_1, \Phi, \varphi_2$		
Cube	$\{001\}\langle 100\rangle$	C	0	0	0	45	0	45
Rotated cube	$\{001\}\langle 110\rangle$	H	135	0	135	0	0	45
	$\{111\}\langle 110\rangle$	E_1	90	55	135	0	55	45
	$\{111\}\langle 110\rangle$	E_2	150	55	135	60	55	45
	$\{111\}\langle 11\bar{2}\rangle$	F_1	120	55	135	30	55	45
	$\{111\}\langle 11\bar{2}\rangle$	F_2	0	55	135	90	55	45
	$\{112\}\langle \bar{1}10\rangle$	I	35	90	135	0	35	45
Goss	$\{110\}\langle 001\rangle$	G	0	90	135	90	90	45

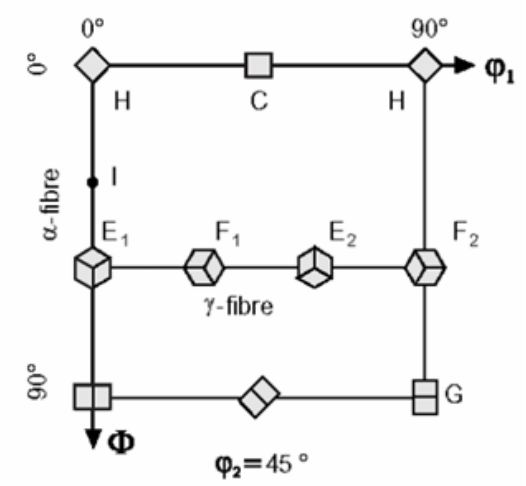

Figure 4. Texture components in rolled bcc metals displayed in Φ_1-Φ,Φ_2= 45 deg section of the ODF. The relative orientations of the cube is illustrated in Table 3 [19].

C. Research on Rolled Nb Sheets

Rolled bcc metals have received less attention, than fcc metals relatively speaking and most of the bcc rolling research is on steel sheets.

1. Vandermeer and Ogle [20-21]

This work shows texture developments in rolled RRR Nb sheet. The pre rolling schedule for the study is shown in Figure 5. As the billet was large grained it was refined to a finer grain size to mitigate the influence of the initial structures. The samples were then rolled, interestingly the samples were cooled with liquid nitrogen between passes, and the whole operation of rolling was done such that the temperature was always kept below 0^{o}C. This was possibly done to prevent significant temperature affects during the study. The samples were taken at different stages of rolling. Results indicate that texture between the surface and center does not vary much from until ~90% reduction. It is a fair assumption that as the sheet there is a double shear kind of effect that develops leading to different surface textures .After 90% reduction there is a strong shear kind of texture that develops in the sheets which can be avoided if the rolls are lubricated as the sheet reaches such reduction ratios. The results also suggests that at such high reduction ratios the deformation is non-homogeneous leading to a depth dependent texture difference. A summary of results are as presented in Table 4. Inhomogenities in microstructure that resulted are also depicted in Figure 6, these were attributed to the non-uniform deformation that takes place during rolling.

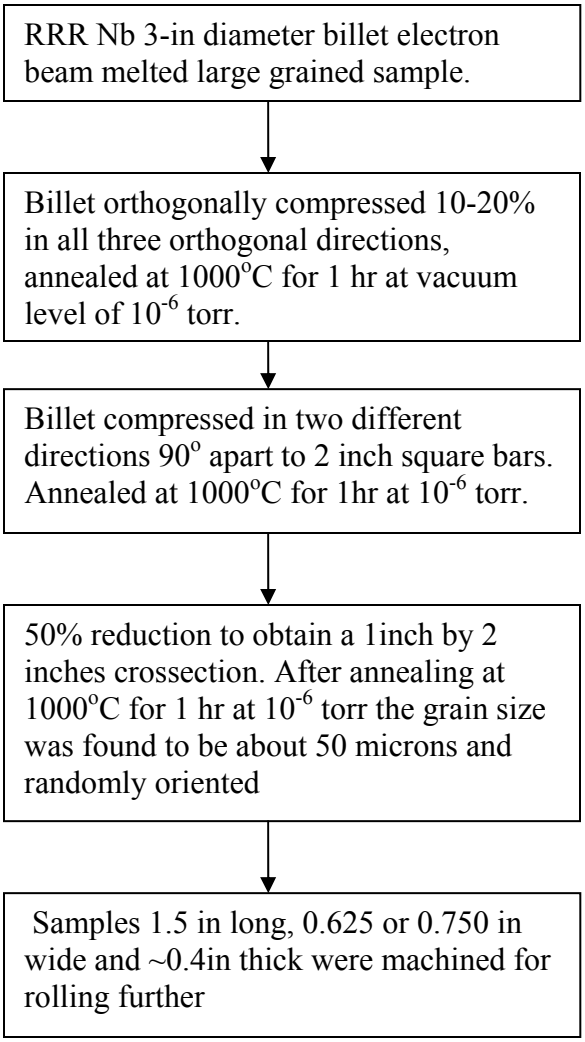

Figure 5. Preprocessing steps to obtain a finer grained microstructure before rolling[20].

Table 4. Summary of texture results on rolled Nb samples through various reduction ratios. [20-21].

Reduction ratio	**Preferred orientations**	**Common fiber description**	**Inhomogenities between surface and center**
<40%	{001}<110> to {111) <110>	Rotated cube and gamma fiber	No
40%-87%	{111}<112> to {112} <110> and {001} <110>	Alpha ,gamma fiber and rotated cube	No
>87%	{110}<113> on the surface, {112} <110> in the center and {001} <110>	Goss and rotated cube at the surface and gamma fiber and rotated cube in the center	Yes

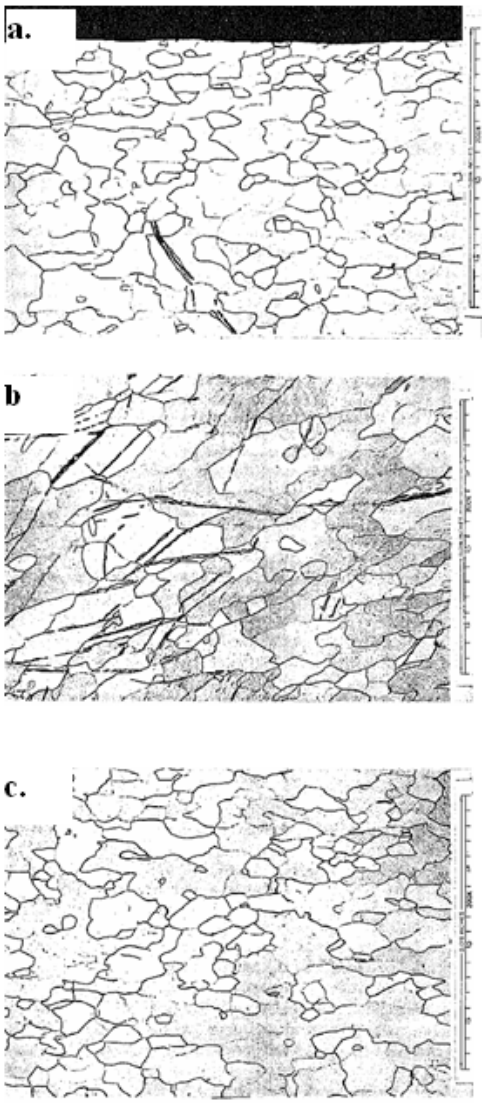

Figure 6. Optical micrographs of the microstructure of rolled Nb a. from the surface, b. from the intermediate section and c. from the center. The rolling direction points to the right for all samples. The scale bar is on the right side reads 0.18in [21].

2. Jiang H et al.[22-24]

The experimental procedure involved single directional rolling of Nb sheet at room temperature in the absence of any lubrication. The sheets were rolled from 2mm thick to 0.7mm thick in six passes. Samples were taken at different reduction ratios and analyzed for the evolution of texture. Annealing was done at 750^{o}C for 1hr in vacuum. The results

of this study suggests that at about 70% reduction there is a texture change from {001}<120> to an incomplete gamma fiber. The gamma fiber seems to strengthen with the reduction and annealing seems to enhance the gamma fiber component. The surface still had strong {001} rotated cube components even after 90% reduction..

3. Sandim et al. [25,26]

The following works mainly deal with rolling a Nb bi-crystal and large grained Nb. This is generally not the preferred way for manufacture of Nb sheet for fabrication applications because the deformations are grain orientation dependent and it is very difficult to break down the microstructure into finer grains starting with very large grains[9]. In the bi-crystal study a 10mm thick bi-crystal with grain orientations (221)[434] and (102)[101] was cut. Rolling these samples and observing the morphology of the grains led to the following conclusions:

Different orientations behaved different under identical rolling conditions resulted in orientation dependent grain boundary character. Grain A showed low misorientation boundaries for 50% reductions. Some high angle boundaries appear in the microstructure. Grain B showed a microstructure containing high angle grain boundaries even at low reductions. Figure 7 shows the morphology of the two grains at a reduction ratio of 70%. Annealing studies on these samples indicated that the final microstructural dependence on the initial orientations.

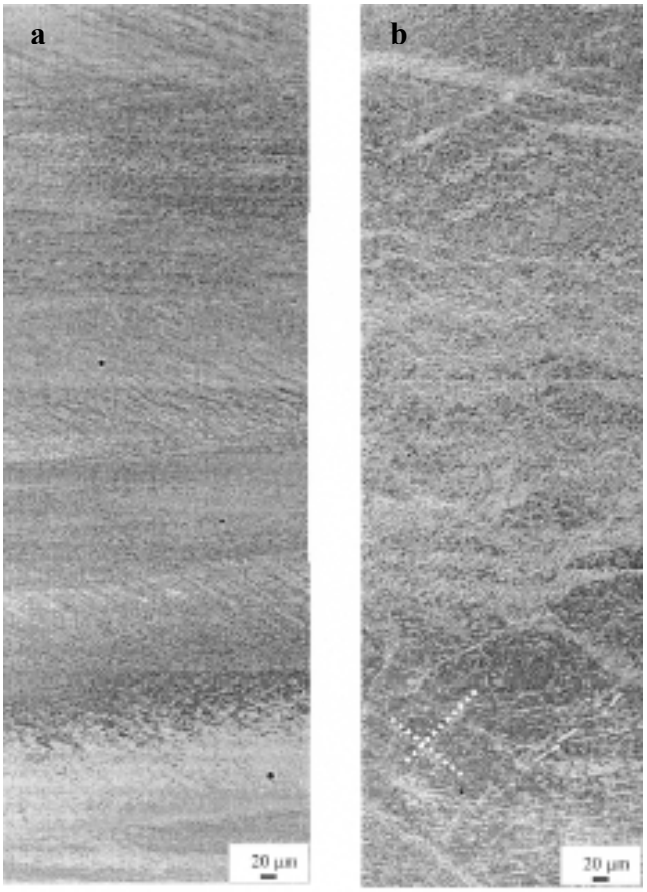

Figure 7. The microstructure of as worked Nb bi-crystal after 70% reduction. a. Grain A and b. Grain B [25].

Grain size differences were observed based on the texture that evolved during annealing Grain B showed a {051}<41-3> texture whereas Grain A showed a strong {021}<501> and weaker {013}<9-41> . Figure 8 shows the difference in annealing behavior with respect to orientation of the grains. The study in [26] confirms the grain size dependence on the texture that is observed in rolling Nb. However, the exact dependence of the grain size with respect to texture is not well understood.

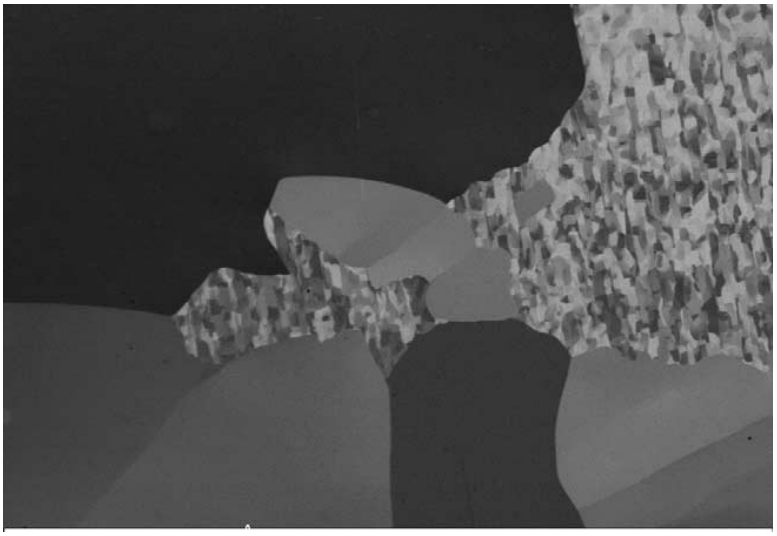

Figure 8. Channeling contrast micrograph of a partially recrystallized specimen 33% deformed annealed at 800^{o}C for 1h in vacuum [26].

A summary of the three studies suggest that:

a. Textures in rolling are dependent on the history of the rolled samples, the way rolling is done and rolling paramets.
b. Total strain seems to have an impact on the texture that develops.
c. Grain sizes are related to annealing textures for the same heat treatment conditions.

D. Radio Frequency (RF) Cavities

1. Introduction

Present day particle accelerators which form a important component of particle physics are based on linear accelerator technologies. They are based on applying time varying fields to accelerate charged particles. Present day high energy accelerators adopt a rf field to create a standing wave which gives the push to accelerate the charged particle

[27,28]. Present day accelerators are designed to produce energies in the order of Giga Electron Volts [27]. Some examples of such high energy colliders are at CERN Switzerland, Jefferson Lab USA to name a few. The International Linear Collider (ILC) is an ambitious collaborative project which involves a dozen countries to build the largest and most powerful linear collider to unravel new particles. When operative the ILC is supposed to produce GeV's of energies, which is comparable to the energy that was supposedly produced during the big bang [29]. Figure 9 depicts the geometry of a RF cavity which forms the heart of these particle accelerators.

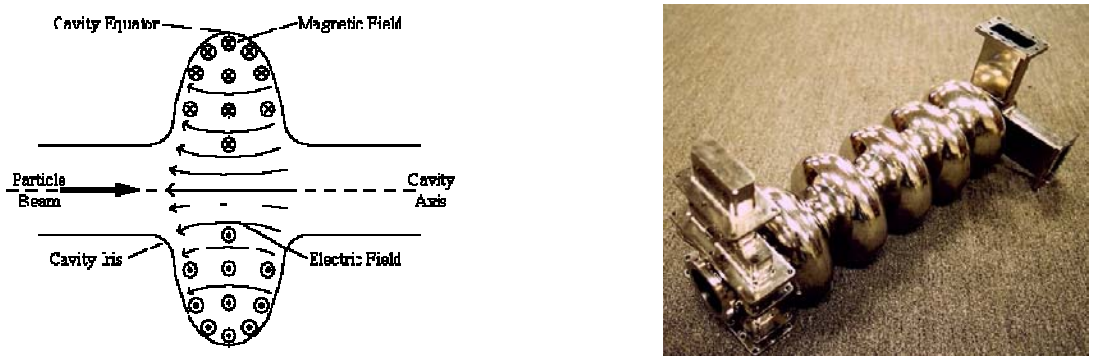

Figure 9. a. Geometry of the cavity along with the fields that act on the particle inside the cavity [28]. b. A five cell cavity, Courtesy: Cornell-LEPP [28].

To produce high energies, high electric fields are required and hence losses need to be at a minimum. Hence, these powerful accelerators are based on superconducting technologies to minimize dissipative losses.

Nb is an ideal candidate for these cavities as it has a high critical temperature of 9.2K below which it is superconducting, it operates at high RF's with very less surface resistance of about 10^{-7}-10^{-8} Ω. The surface resistance of Nb compared to other metals

and compounds is as shown in Figure 10. Apart from this it is technologically feasible because of the ready availability, workability, appreciable thermal conductivity and stable superconducting properties. However, defects in raw material has impeded the attainment of theoretical limits of electric field value attainable for Nb[27].

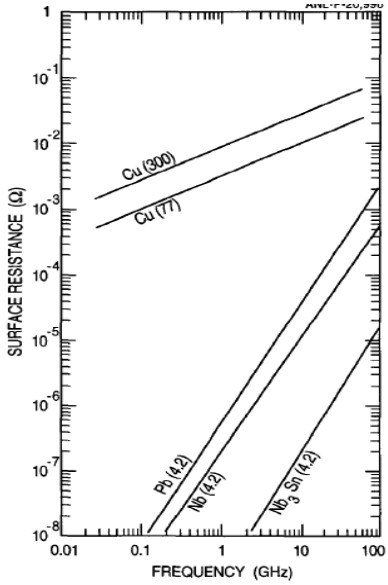

Figure 10. Variation of surface resistance with frequency of various superconducting materials at frequencies typical to that of RF cavities in comparison with Cu at 77 and 300K. Nb has low surface resistance in the operating range of 1GHz among the metals. [27].

2. Fabrication of Niobium SRF Cavities

There are different approaches involved in making superconducting RF cavities. The most common approach is deep drawing of high purity polycrystalline RRR Nb into hemispherical cavities followed by trimming of the edges. Trimming of edges is necessary due to problems associated with the earring behavior observed during the deep drawing operation. After trimming the half cells are electron- beam welded in vacuum to form an elliptical cavity. Then the cavity is shape adjusted and undergoes a series of

cleaning operations, which is the critical step needed to obtain the necessary performance. Contamination is a primary concern because RF superconductivity is a near surface phenomenon the surfaces need to be nearly perfect. The effect of different elements on RRR and hence cavity performance are as shown in Figure 11.

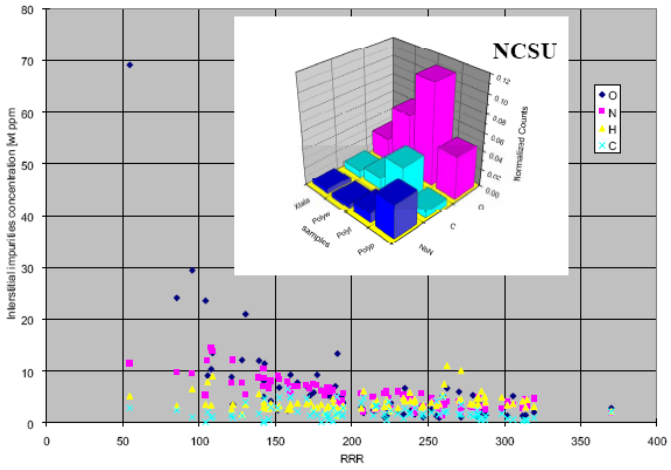

Figure 11. The effect of different impurity content on the RRR value of Nb is as shown. Small variations in impurity contents seem to have a large impact on the RRR values due to creation of local hotspots [30].

Contaminants are introduced during the different stages of fabrication and surface preparation steps. The fabrication procedure involves machining, rolling and annealing [31]. Machining by electro discharge or spark erosion introduces hydrogen and oxygen. Rolling can introduce some interstitial impurities as well [32]. The cleaning procedures involve solutions with high hydrogen ion content which introduces hydrogen into the material. As depicted in Figure 12 a series of heat treatments seem to be the preferred way to remove some of these interstitials.

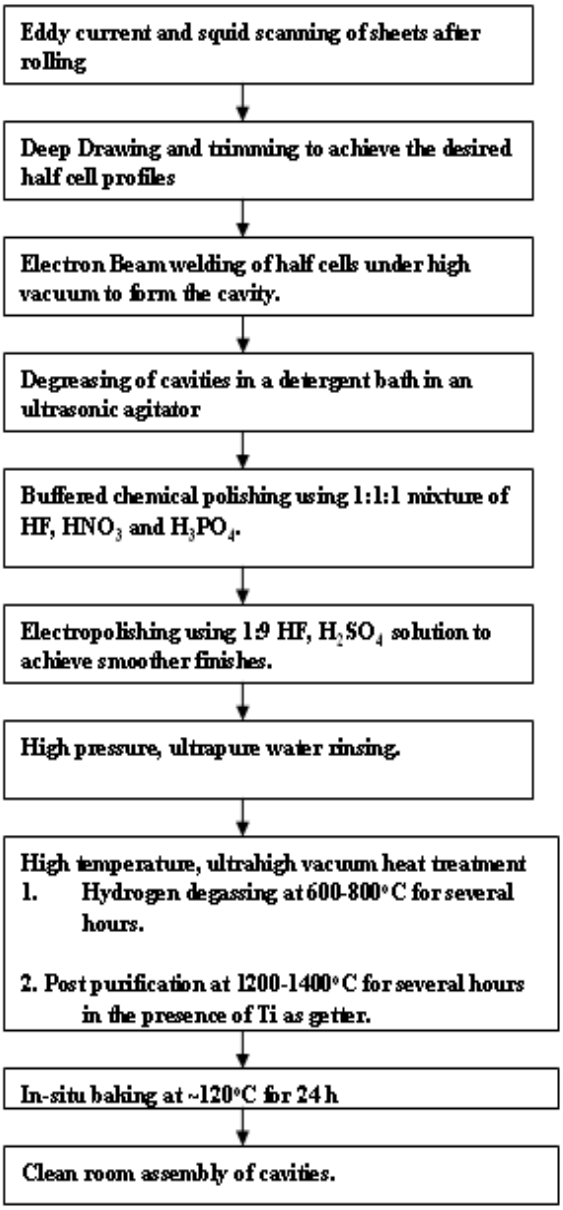

Figure 12. Steps involved in fabrication and assembly of high performance RF Nb cavities[33].

Apart from deep drawing there are other methods used to produce RF cavities these include hydroforming, spinning and explosive forming. Further details of these methods can be found elsewhere [34-38].

All of the above fabrication methods mention the non-unifromity in properties that is observed in the sheet material which can be directly related to the microstructure. Zamiri et al.[39] have discussed some of the effects that are caused by the unfavorable microstructures in these precursor Nb sheets by conducting bulge tests on specimens. Figure 13 shows examples of non-uniform microstructure seen in commercial sheets.

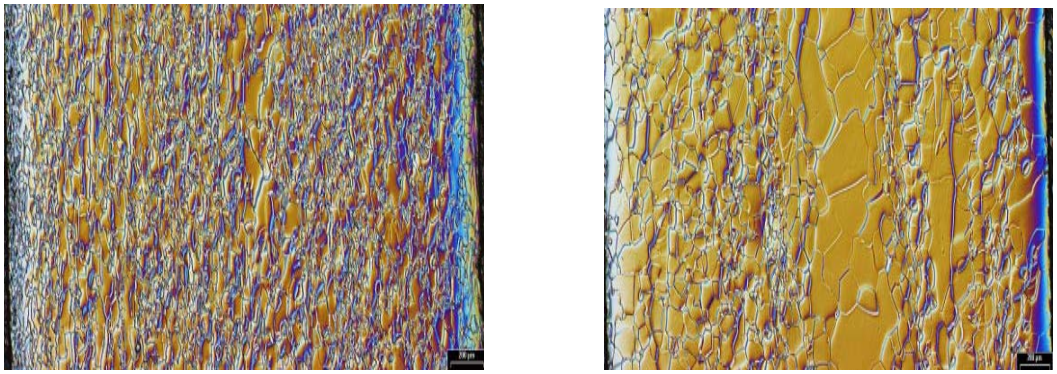

Figure 13. Typical microstructure observed in commercial Nb. These non-uniformities lead to variable deformation characteristics and poor formability [38]. The microstructures are from different sections of the same sheet.

3. Fine Grain Cavities versus Single Crystal and Large Grain Cavities

In 2005 Kneisel et al. [19] produced a cavity made from a large grain/single crystal Nb, this material was found to have superior mechanical and niobium superconducting properties. The production of this prototype cavity involved EDM slicing of a large grain grain/single crystal and following the fabrication procedure mentioned in Figure 12.

The main advantages for using large grain/single crystal over fine grain material are:

a. Polishing results are repeatably better in large grain and single crystal.
b. The ability to manufacture such material will cut down on fabrication steps and cost

It was widely believed that grain boundaries have a detrimental effect on the performance of an SRF cavity, in terms of the quality factor [27]. A performance study of cavities with different grain sizes indicates no significant change in the performance of the cavity in terms of the quality factors[21] and speculates that the drop in the quality factors has to do more directly with the impurities introduced rather than the effect of grain boundaries.

3.1 Mechanical Testing on Single Crystal/Large Grain Cavity Material

On going studies [30] on large grain and single grain material presented a unique problem with the forming of these cavities. Figure 14 shows the tensile test results of single grains in different orientations. The ductility is as high as 100% suggesting excellent formability. However, the same material under a two-dimensional test like the bulge test shows poor formability. The results of the bulge test comparing the formability of large grained material with fine grained material is as shown in Figure 15.

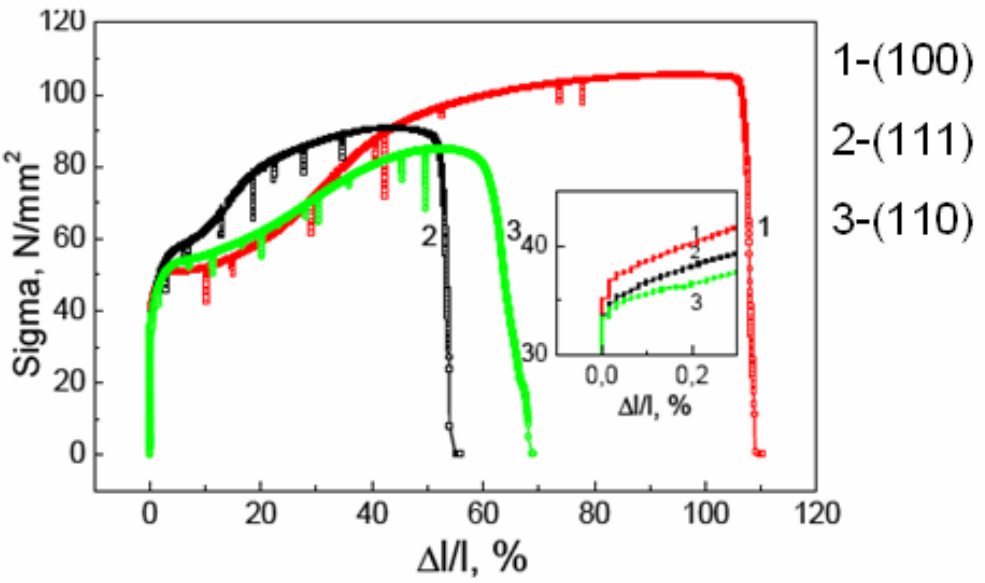

Figure 14. Tensile tests of crystals in different orientations indicate the anisotropy in tension in different directions in Nb [30].

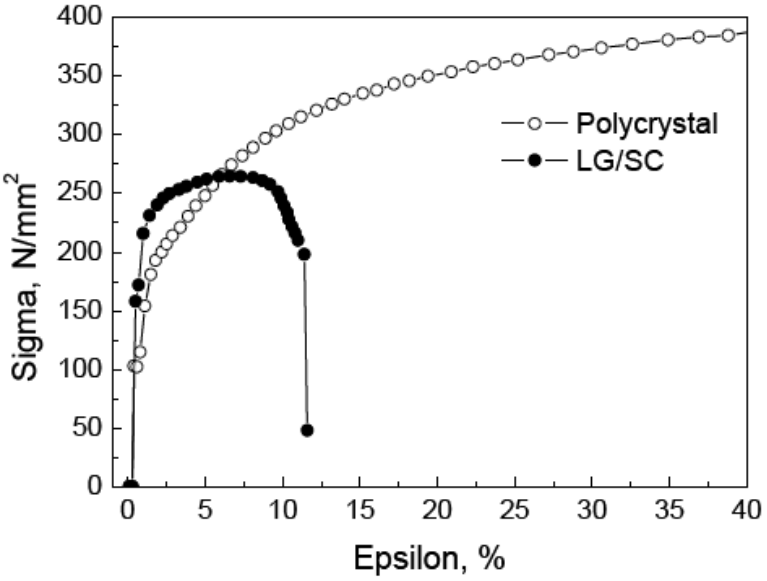

Figure 15. Biaxial bulge test indicates a poor formability with the large grain/single crystal material than a poly crystal sample [30].

E. Equal Channel Angular Extrusion (ECAE)

From the above sections it can be seen that incomplete breakdown of initial microstructures and inhomogenities in the starting material leads to undesirable deformation characteristics which is reflected in the works of Zamiri et al.[39].

ECAE is based on the the principle that simple shear deformation is an effective and preferable way of bulk deformation[40-42]..

ECAE as a deformation technique was the brainchild of V.M Segal[43]. It consists of passing a billet through a well lubricated intersecting die, creating a region of uniform simple shear as the billet passes the die. The usual intersecting die angles are 90^o,120^o and 150^o. Figure 16. illustrates a 90degree die setup with the planes referenced in conventional terminology. As it can be seen from the figure the intial and final crossections of the billet does not change. Multiple passes of ECAE refers to passing the billet through the intersecting channels more than once. High strains can thus be introduced into the billet.

The strain is expressed by [44]:

$$\epsilon = (2N/\sqrt{3})\cot(\Phi) \quad \text{.....(4)}$$

Where: N is the number of passes(1,2,3…)

2Φ is the die angle (90, 120 or 150 commonly used).

For a 90^o die the strain per pass is 1.15.

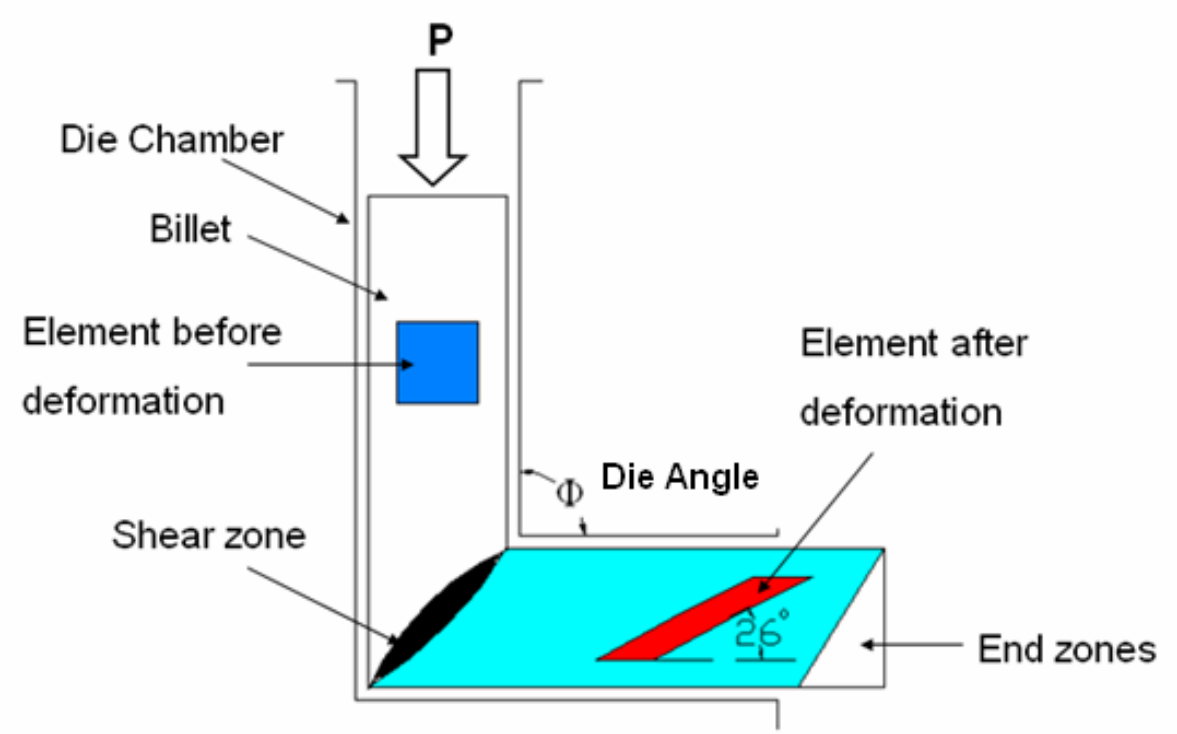

Figure 16. Illustration of a 90^{o} ECAE setup. The deformation element is as shown after one pass.

Relations involving strain per pass, equivalent reduction ratio and equivalent area reductions were derived by Segal [44]. These relations are a way ECAE can be compared with other bulk deformation processes. Table 5 summarizes the parameters for multi pass ECAE with a tool die angle of 90^{o}.

Table 5. Theoretical strain and other parameters for mulipass ECAE [44].

Number of passes	**Total Strain intensity (ϵ_n)**	**Equivalent reduction ratio (RR)**	**Equivalent area reduction (AR) %**
1	1.15	3.2	69
2	2.31	10.2	90
3	3.46	32.7	97
4	4.62	105	99
5	5.77	335	99.7
6	6.93	1073	99.9
7	8.09	3436	99.97
8	9.24	10100	99.99

Effective breakup of the microstructure by ECAE has been demonstrated [45-47].

Depending on the rotations provided in between passes in multi pass ECAE (mECAE), mECAE processing routes are defined as follows.

Route A- No rotation of the billet between passes.

Route B- Rotations of alternating 90^o between passes.

Route C- Involves 180^o rotation between passes.

Route B_c- Rotations of $+90^o$ between passes

Route E – This is a hybrid route which corresponds to Route C but with a 90^o rotation after even number of passes.

Different routes have their unique features and deformation characteristics.

More information on the routes and the microstructure can be found in the following references [45,48-49].Texture evolution has been studied over the years and can be found in these references[50-55].

1. ECAE of Niobium

Previous work on ECAE of Nb done at Texas A&M [56,57] has shown the effective breakdown of microstructure, however there seemed to be issues related to banded microstructures. With proper pre-processing and control of heat treatments these can be overcome

ECAE processed bulk Nb rolled into sheet has showed interesting textures[56,58]. ECAE is an effective tool to exercise control over the microstructure, in terms of breaking down the microstucture and contol over the textutre that can be obtained. ECAE of bi-crystal Nb can be found in the work of Sandium et al.[59]

CHAPTER III

MATERIALS AND METHODS

A. Raw Material

The raw material used in the study were RG and RRR Nb bars. RG bars were used to evaluate the influence of the impurity level on the microstructural evolution with the hope that behavior similar to that seen in RRR Nb could lead to cost savings for material used for repeat experiments. The raw material was supplied by ATI Wah Chang. The impurity levels of the material studied are as shown in Table 6. The major impurity content difference is substitutional Ta. The bars came from ingots that were electron beam melted to obtain the two purity levels and then water jet cut as could be seen from the surface of the surface of the extrusion billets. The initial grain sizes are on the order of centimeters The samples were not macro etched prior to ECAE to reveal the grains. Indications of large initial grain sizes were evident after the first preprocessing step where the deformation appears to be inhomogeneous in most cases. Grain boundaries were observed in some cases as boundaries between regions showing very different deformation behavior.

Table 6. Impurity content in ppm of RG and RRR Nb used for the current study. The concentrations were reported by ATI- WahChang (Nb supplier).

Element	Concentrations are in ppm	
	RG	RRR
C	<20	<20
Fe	<10	<25
H	<10	<3
Hf	Na	<50
Mo	<50	<30
N	<10	<20
Ni	<20	<20
O	<30	<40
P	NA	<30
Si	<20	<25
Ta	<2000	<350
Ti	<13	<40
W	<50	<30
Y	NA	<2
Zr	<7	<50
Al	<10	NA
Cr	<30	NA
S	<10	-

The billets were EDM cut to nominal dimensions 25.4 mm x 25.4mm x 254mm. The RG and RRR bars were sectioned as shown in Figure 17. Table 7 mentions the processing plan and the test matrix for the study.

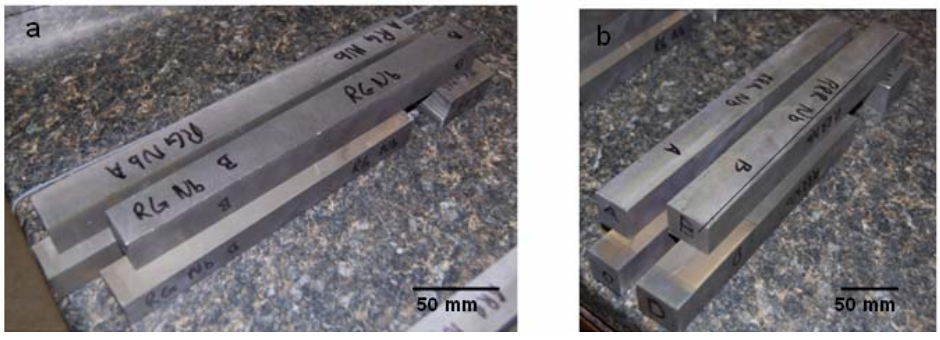

Figure 17. a. Four RG Nb bars used in the study. b. 4 RRR Nb bars used in the study. The bars were sectioned using a wire EDM and are nominally 25.4mm square.

Table 7. Processing plan for the Nb study.

Purity level	Billet Id	Preprocessed	ECAE	Post ECAE			
				Bars cut in half	Sheet Id (Sample to be rolled)	Heat treatment	
RG	A	√	4A	RGA1	RGA1LA	As worked	
					RGA!LB	Full Anneal	
				RGA2	RGA2FA	Partial Anneal	
					RGA2FB	As worked	
	B	√	4Bc	RGB1	RGB1LA	As worked	
					RGB1LB	Full Anneal	
				RGB2	RGB2LA	Partial Anneal	
					RGB2LB	As worked	
	C	√	Saved				
	D	√					
RRR	A	√	4A	RRRA1	RRRA1LA	As worked	Cross Rolling
					RRRA1LB	Full Anneal	
				RRRA2	RRRA2FA	Partial Anneal	
					RRRA2FB	As worked	
	B	√	4Bc	RRRB1	Saved		
				RRRB2	RRRB2FA	Partial Anneal	
					RRRB2FB	As worked	
	C	√	4E	RRRC1	Saved		
				RRRC2	RRRC2FA	Partial Anneal	
					RRRC2FB	As worked	
	D	√	4Bc	RRRD1	RRRD1LA	As worked	
					RRRD1LB	Full Anneal	
				RRRD2	RRRD2FA	Partial Anneal	
					RRRD2FB	As worked	

B. ECAE Procedures

1. ECAE Routes

The ECAE processing routes chosen for the study were Route A, Route B_c and Route E. All the billets underwent four pass ECAE because it was previously shown that four passes of ECAE is sufficient to breakdown the microstructure.

a. Route A- This route is expected to give the highest texture after processing. However, the yield with this route is low and the worked material needs careful identification.
b. Route B_c- This is route is often repeated to be the most effective for breakdown of the microstructure. The textures produced following this route are uniformly distributed, with no strong components.
c. Route E- This is a hybrid route, it also effective for breakdown and softening of texture components. The main advantage of route 4E is higher fully proceseed material yield than compared to route $4B_c$.

2. Pre-Extrusion and Extrusion Procedures and Conditions

Results of the study done by Bryant [57] forecast banding in the ECAE processed and annealed microstructures. This is attributed to large grains and texture inhomogenities in the starting microstructure. Hence, prior to processing the billets via the different ECAE routes, the material was preprocessed using multipass ECAE. Preprocessing consisted of five ECAE passes plus recrystallization. The microstructures produced by this processing were uniform as shown in Figure 18. The average grain sizes was ~ 20-30 μm with low texture components..

The billets were then extruded as indicated in the test matrix. Each billet had the id marked on one of the faces as shown in Figure 19 shows a schematic of a typical billet, with the nomenclature used throughout this report .All the extrusions were done in a 90^{o} die at room temperature with a punch speed of 5mm/sec. A lubricant was used to reduce friction between the billet and the die walls. After all extrusions were completed the billet end zones were removed, reducing the billet length from ~254 mm to ~200mm. Billets were sliced into halves and samples cut for microstructural characterization. All the cutting done in the study was done using EDM unless specified otherwise. The reasons for using the EDM is:

a. little material loss

b. microscopic heat affected zone

c. microscopic mechanical damage zone

d. a flat clean surface.

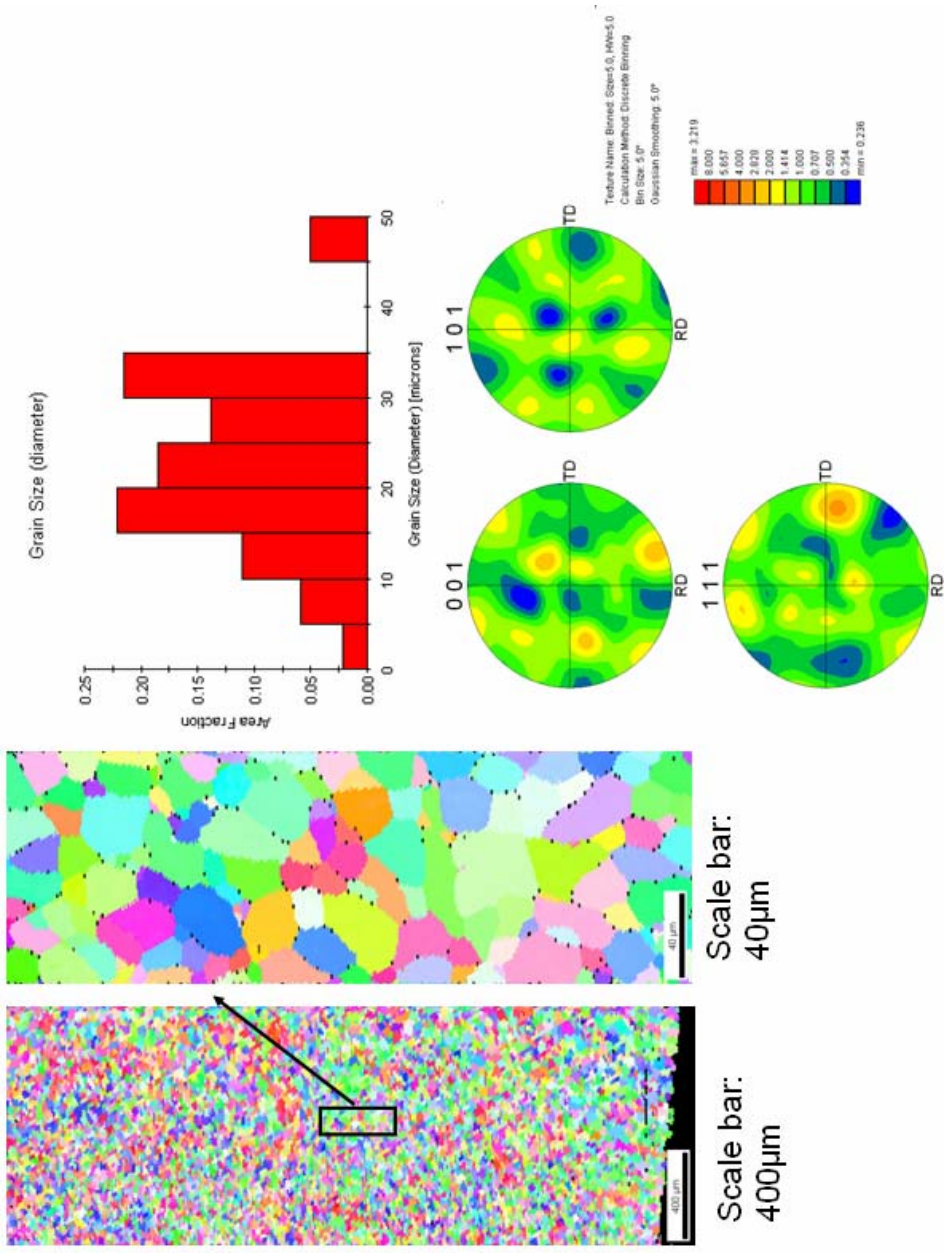

Figure.18. Microstructure of a preprocessd billet RG-D. The OIM map is of the tranverse plane with the extrusion direction coming out of the plane of the paper.

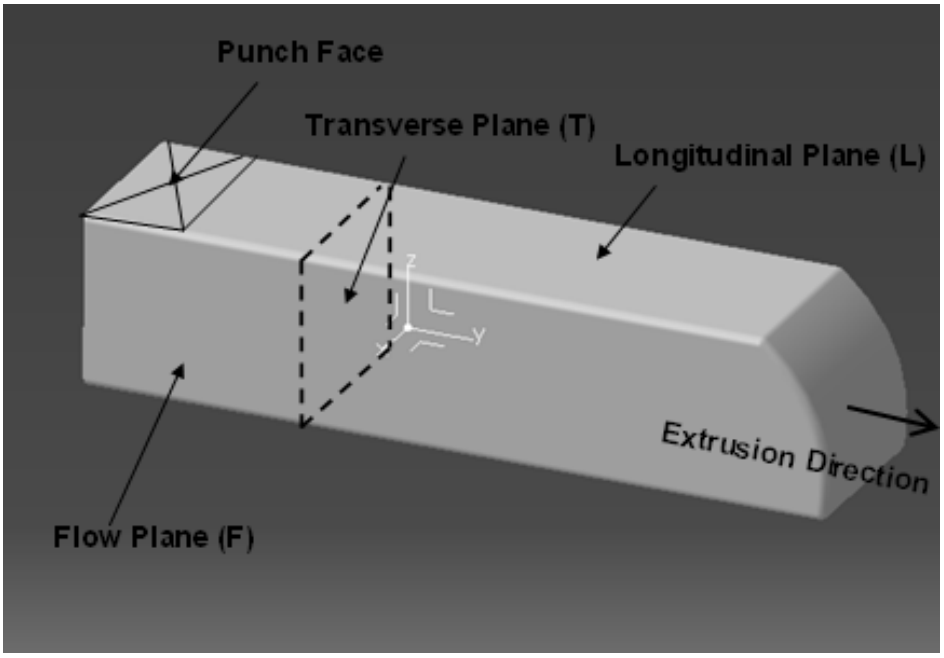

Figure 19. Schematic of an ECAE processed square cross section with the principal planes identified.

3. Billet Slicing and Naming Convention

The samples processed had to be cut in half lengthwise for the rolling because rolling of the square bars was problematic in the cross direction..The billets were sliced as shown in Figure 20. The naming convention was as follows : 1. the first two or three letters designate the purity level RG or RRR; 2. then the billet is identified; 3. then the side of the billet is identified as to whether or not it contains punch face or not; 4. then follows the way the billet was sliced reducing to thin the bar thickness. A or B indicates whether the billet slice came from the top (A) or bottom (B) side of the billet with respect to the last extrusion

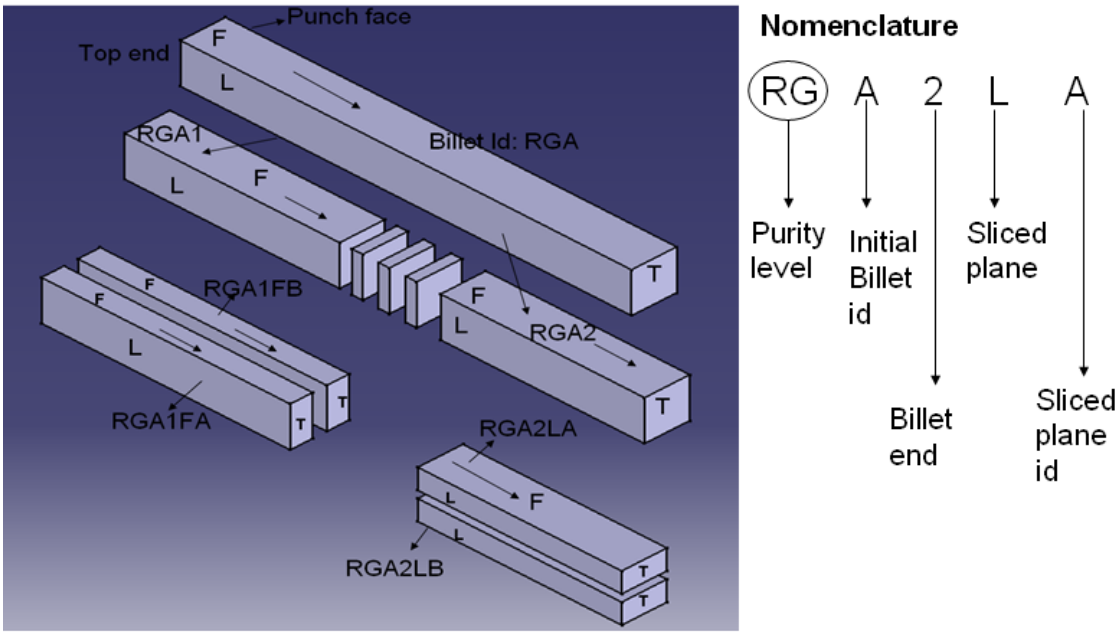

Note: The punch face is opposite to the face marked L.

Figure 20. Cutting and naming scheme for the billet. The sliced billet was cross rolled.

C. Heat Treatments

Niobium oxidizes rapidly at temperatures above about 300^{o}C. Hence all heat treatments are under vacuum. For the smaller samples (used for recrystallization curves), a diffusion pump vacuum furnace at TAMU was used. This could reach vacuum levels of 10^{-6} - 10^{-7} torr dynamic vacuum. The furnace is coupled with an Omega controller and the reading is obtained with a K-type thermocouple which forms a needed link in the closed loop temperature control system.

The furnace is on rails and can be slid so that the quartz tube is in the furnace as soon the furnace reaches the desired temperature. When the cooler quartz tube is in the furnace a drop in temperature of approximately 20-40^{o}C is observed depending on the furnace temperature. However the desired temperature (within a range of ± 2^{o}C) is reached within five to ten minutes and only after this the the heat treatment time clock is started.

The larger billet samples were heat treated at AMES DOE lab; a dynamic vacuum level of approximately 10^{-6} torr was maintained at AMES for each heat treatment.

D. Metallographic Sample Preparation

1. Billet Cutting

For the billet/slab samples either the EDM or a diamond saw was used to cut up samples. The sheet samples were cut using a hand shear. Using the hand shear is the not the best way to cut these samples. Even though they are faster to cut, they require polishing to deeper levels to negate the surface deformation produced by the hand shear.

The best way to cut the sample is to use a diamond saw. It introduces the least surface deformation.

2. Mounting of Specimens

The mounting procedure used is a hot mounting procedure using a Buehler Micromet equipment. The sample is first placed on a stage and bakelite powder hot pressed (maximum nominal temperature reached was 150^{o}C)at a pressure of 6-8 kips using a spring loaded cap for about 15 minutes. The sample was removed from the hot mounting press and engraved with the sample ID.

3. Polishing Procedures

The polishing procedure followed is as described below:

a. Grind the mounted specimen flat with 420 grit SiC paper using running water as the lubricant and to remove the polishing debris .

b. The sample was then ground using a 600 grit SiC paper for approximately 3minutes

c. Grinding was continued with 800 grit SiC paper and water followed by 1000 grit SiC paper Polishing time varied between 10-20 minutes during this step.

d. Diamond pastes of 9 μm and 3 μm were then used to polish the sample. An oil based lubricant was used during this stage. Care was taken to use minimum quantities of the paste because diamond particles have a tendency to embed in the sample leading to pits. The pressure applied during this stage was significantly less compared to the first two steps. The time taken during this step was around 10 minutes.

e. Final polishing was done on a lapping cloth with 0.05 μm silica suspension in water. A polished surface looks scratch free under a microscope at 500x and has a mirror finish. Depending on the surface after inspections under a microscope the time taken during this stage varies between 15-30 minutes.

E. Etching Procedure

The etching procedure used was a general microscopic etching procedure for refractory metals. The etchant consisted of 1:2:2 volumes of HNO_3, HF and lactic acid. Etching is generally done by swabbing the surface of the polished sample with a cotton swab for 15-30 seconds during etching. Dipping the sample with the mount in the acid can lead to contamination and a large surface area for reaction leading to inefficient usage of the etchant. Once etched the sample were cleaned with water and methanol and dried completely. Over etching leads to burnt looking surfaces and requires repolishing. Extreme precaution must be ensured and safe practices must be followed as the acids dealt with are extremely corrosive in nature..

F. Hardness Tests

Vickers microhardness tests were conducted on the polished samples. The samples were mounted onto a universal stage of the microhardness tester. A load of 300g for 13 sec was applied. Experiments indicated that lower loads may give false significantly different results as the sampled area may not be representative or surface affects overly influence the measurements. We have found that Vickers hardness measurements tend to

level off after 200 gms on a polycrystalline sample with an average grain size <30 μm. For ultafine grained sample, and a well polished surface lower loads may work fine.

G. Rolling

Rolling was carried out at ORNL. Some of the samples that were EDM machined to be rolled had a slight taper and had to be upset slightly to flatten the thickness. The rolling reductions for the initial passes were ~5-10% and for later passes the reductions were in the range 10-20%. Side cracking of the Nb sheets was observed in some cases but the crack did not propagate inwards from the edges. The slabs were rolled from initial thickness of nominally 12mm to about 0.8mm. The total reduction by rolling was ~ 90%. Samples were cut at reduction ratios of nominally 50%, 70% and 90% for analysis. All the rolling was done at room temperature Table 8 (attached at the end of the chapter) presents the rolling data for all samples.

H. Tensile Tests

The specimens used for the tension tests were pin loaded test specimens as per ASTM standard E 8-04. This standard is for sheet type specimens. The dimensions of the sample are shown in Figure 21. Tension test samples were cut from the sheet material at orientations of 0^o, 45^o and 90^o to the final rolling direction.

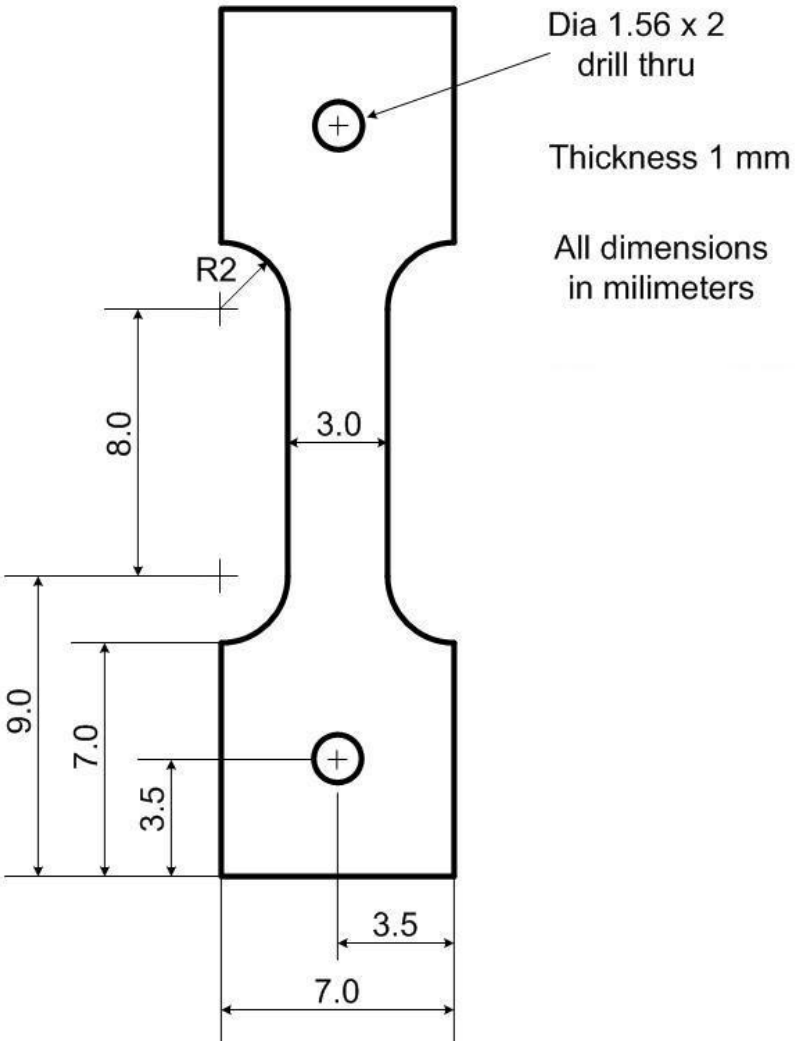

Figure 21. Specimen dimensions used for the tensile tests. This geometry follows ASTM E-8-04, for sheet type specimens.

The samples were EDM cut and then drilled to obtain the specimens. The tension tests were done using a MTS load frame with special grips to hold the samples. An extensometer with a 40% range was used to measure the strain. The samples were tested to failure. The initial and final width and thickness dimensions were noted.

I. Texture Analysis

All the texture analysis was done at MSU, by a fellow colleague Derek Baars. The procedure followed as described by Baars is: "Sheet samples were cut, mounted, and their cross sections mechanically polished to 0.05 μm with colloidal silica for a mirror finish. Orientation imaging microscopy (OIM) scans were conducted on a Camscan 44Fe SEM using a TSL (Link) system. Each scan spanned the entirety of a sheet sample's cross section, with 4 μm between data points. Inverse pole figure OIM maps, pole figures, and orientation distribution functions (ODFs) were made to examine each sample's crystallographic texture; grain size and grain aspect ratio were also determined using a TSL OIM Analysis v5.2".

Table 8. Rolling data showing the reduction after each pass.

Sheet ID	Starting Thickness	Pass 1	Pass 2	Pass 3	Pass 4	Pass 5	Pass 6	Pass 7	Pass 8	Pass 9	Pass 10	Pass 11	Pass 12	Pass 13	Pass 14	Pass 15	Pass 16	Pass 17	Pass 18	Pass 19	Pass 20	Pass 21	Pass 22	Pass 23
	All dimensions in mm																							
RRRD1LB	13.77	12.42	11.20	10.11	9.12	8.18	7.39	6.68	6.17	5.59	4.70	4.01	3.53	2.95	2.39	1.96	1.65	1.37	1.17	1.07	0.84			
RRRA2FA	13.18	12.42	11.25	10.19	9.17	8.20	7.42	6.71	6.17	5.56	4.72	4.04	3.53	2.95	2.41	1.98	1.65	1.40	1.24	1.07	0.89			
RRRB2FA	13.46	12.45	11.23	10.16	9.17	8.23	7.42	6.71	6.25	5.69	4.78	4.04	3.58	3.05	2.44	1.98	1.73	1.47	1.22	1.12	0.89			
RGB1LB	13.34	12.45	11.25	10.19	9.19	8.26	7.44	6.73	6.22	5.64	4.80	4.06	3.56	3.00	2.46	2.03	1.75	1.42	1.22	1.04	0.91			
RGA2FA	13.21	12.45	11.28	10.19	9.19	8.26	7.47	6.73	6.30	5.69	4.80	4.06	3.63	3.05	2.46	2.03	1.70	1.47	1.27	1.09	0.94			
RRRC2FA	13.00	12.40	11.20	10.16	9.17	8.23	7.44	6.71	6.25	5.66	4.75	4.06	3.56	3.00	2.44	2.01	1.70	1.42	1.24	1.07	0.97			
RRRD2FA	12.73	12.45	11.20	10.16	9.17	8.23	7.44	6.71	6.17	5.61	4.75	4.06	3.51	2.97	2.46	2.01	1.68	1.37	1.24	1.04	0.94			
RGA1LB	12.40	12.40	11.20	10.21	9.25	8.28	7.47	6.76	6.22	5.69	4.80	4.09	3.58	3.00	2.49	2.03	1.70	1.42	1.24	1.07	0.94			
RRRA1LB	12.57	11.48	10.54	9.42	9.04	7.92	7.44	6.58	6.25	5.74	4.85	4.17	3.61	3.07	2.52	2.11	1.78	1.50	1.35	1.12	0.99			
RGB2FA	12.57	12.40	11.23	10.21	9.22	8.26	7.47	6.73	6.17	5.61	4.78	4.11	3.53	2.97	2.52	2.03	1.70	1.40	1.22	1.07	0.91			
RRRC2FB	11.86	12.04	11.25	10.26	9.27	8.31	7.49	6.78	6.12	5.77	5.03	4.19	3.56	3.10	2.57	2.11	1.73	1.52	1.37	1.14	1.02	0.89	0.71	
RGB2FB	11.84		11.30	10.29	9.30	8.36	7.54	6.83	6.17	5.72	5.00	4.22	3.63	3.07	2.54	2.13	1.80	1.50	1.30	1.17	1.02	0.89	0.79	
RGA1LA	11.38		11.28	10.31	9.32	8.38	7.57	6.83	6.17	5.79	5.08	4.22	3.61	3.10	2.59	2.13	1.78	1.60	1.40	1.17	1.02	0.97	0.76	
RRRA1LB	11.38		11.07	10.03	9.14	8.23	7.42	6.71	6.02	5.56	4.85	4.09	3.48	2.95	2.49	2.03	1.63	1.42	1.22	1.02	0.91	0.74	0.64	
RRRD2FB	11.10		11.02	10.26	9.25	8.33	7.52	6.78	6.12	5.66	4.93	4.19	3.58	3.02	2.46	2.11	1.75	1.45	1.24	1.14	0.97	0.84	0.74	
RRRB2FB	1.09		11.02	10.24	9.25	8.31	7.52	6.78	6.12	5.82	5.08	4.17	3.56	3.12	2.64	2.11	1.75	1.57	1.37	1.14	1.04	0.89	0.76	
RGB1LA	10.41		10.39	10.21	9.30	8.31	7.54	6.83	6.17	5.56	5.00	4.39	3.63	3.02	2.57	2.11	1.78	1.37	1.37	1.17	1.04	0.89	0.81	0.58
RRRD1LA	10.21		10.26	10.13	9.25	8.31	7.49	6.78	6.12	5.54	4.95	4.32	3.58	3.00	2.51	2.11	1.75	1.47	1.32	1.19	0.99	0.84	0.74	0.64
RRRA2FB	10.16		10.16	10.11	9.30	8.28	7.47	6.73	6.10	5.51	5.00	4.37	3.56	2.95	2.57	2.11	1.75	1.42	1.30	1.17	0.97	0.84	0.71	0.61
RGA2FB	9.83		9.80	9.83	9.22	8.31	7.52	6.78	6.12	5.54	5.03	4.42	3.61	3.00	2.57	2.13	1.80	1.47	1.35	1.17	0.86	0.91	0.74	0.66

The numbers in red indicate cross rolling
The numbers highlighted in orange indicate that samples were cut from the sheet at these steps

CHAPTER IV

RESULTS

The objective of this study was to obtain Nb sheet with good formability. Formability is defined here as deep drawability. We assume that formability is directly related to microstructure. The goals of this study were to correlate the effects of the independent variables on the dependent variables in the study. These variables are listed in Table 9.

Table 9. List of the independent and dependent variables considered in the study.

Independent variables	**Dependent variables**
Purity of sample: a. High Purity (RRR) b. Low Purity (RG)	Grain morphology : Grain size and shape
ECAE Routes (A, Bc, E)	Texture
Intermediate Heat Treatment	Mechanical properties: a. Yield strength b. Ductility c. Ultimate Tensile strength d. Plastic Strain Ratio (r) e. Hardness g. Hardening exponent

A. Recrystallization Behavior

1. ECAE Processed Billets

The annealing behavior of Nb processed by four pass ECAE is as presented for different purity levels (Figure 22) Recrystallization is realized by the initial drop in the hardness value (or ultimate strength) value. The recrystalliziation curves show that recrystallization reaches completion in RRR Nb at a lower temperature of ~800^{o}C as compared to RG Nb which recrystallizes at a higher temperature of about 900^{o}C for the same ECAE processing route A. Comparison between RG samples RGA and RGB which had been processed by ECAE 4A and ECAE 4Bc indicate that the recrystallization behavior depends on the processing route. Route Bc seems to have a higher recrystallization temperature than Route A by ~100^{o}C.

The hardness of the RGA material after four pass ECAE is slightly higher than that of RRRA material by a factor of ~20HV. RGA and RGB have similar starting hardness values (assuming an experimental error of 5%) indicating that the hardness of RRR Nb is lower than that of RG Nb when the material is worked to similar extents. The hardness values of RGA and RGB deviate from one another around the recrystallization temperature indicating that the detailed recrystallization behavior is directly dependent on the ECAE route. Comparing the trends of recrystallization curves RGA and RRRA suggests the annealing behavior between similarly processed materials is different depending on the purity of the sample. Purity appears to be an important component in the recrystallization behavior of the samples.

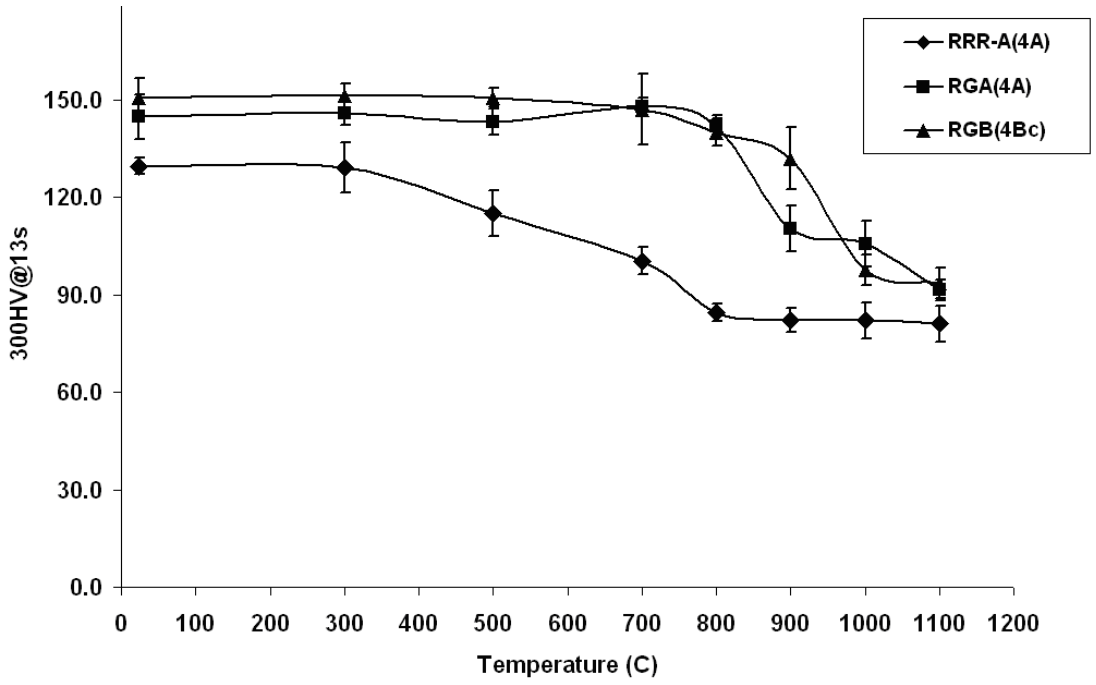

Figure 22. Recrystallization curves of four pass ECAE processed RG and RRR Nb for differents ECAE routes.

Based on these curves the heat treatment temperatures prior to rolling were chosen. The heat treatment temperatures are as shown in Table 10.The term partial recrystallization refers to the heat treatment that will cause a decrease in hardness by ~50%.

Table 10. Heat treatment temperatures selected.

Purity	RRR	RG
Partial Recrystallization	600^{o}C	900 ^{o}C
Fully Recrystallized	750 ^{o}C	1100 ^{o}C

2. ECAE Processed and Rolled Sheets

The recystallization behavior of ECAE processed and rolled sheets is as shown in Figure 23. First, comparing the recrystallization behavior of high purity samples RRRD1LA and RRRD1LB which have been processed by ECAE route 4Bc we have:

a. The initial hardness of RRRD1LA is higher than RRRD1LB by factor of ~50HV. The difference in hardness reflects the influence of the intermediate heat treatment, RRRD1LB had undergone a full anneal after ECAE processing and then cross rolled whereas RRRD1LA was rolled in the as worked condition.

b. The recrystallization curves show similar trends and the recrystallization temperature is about the same ~700^{o}C for both ECAE routes.

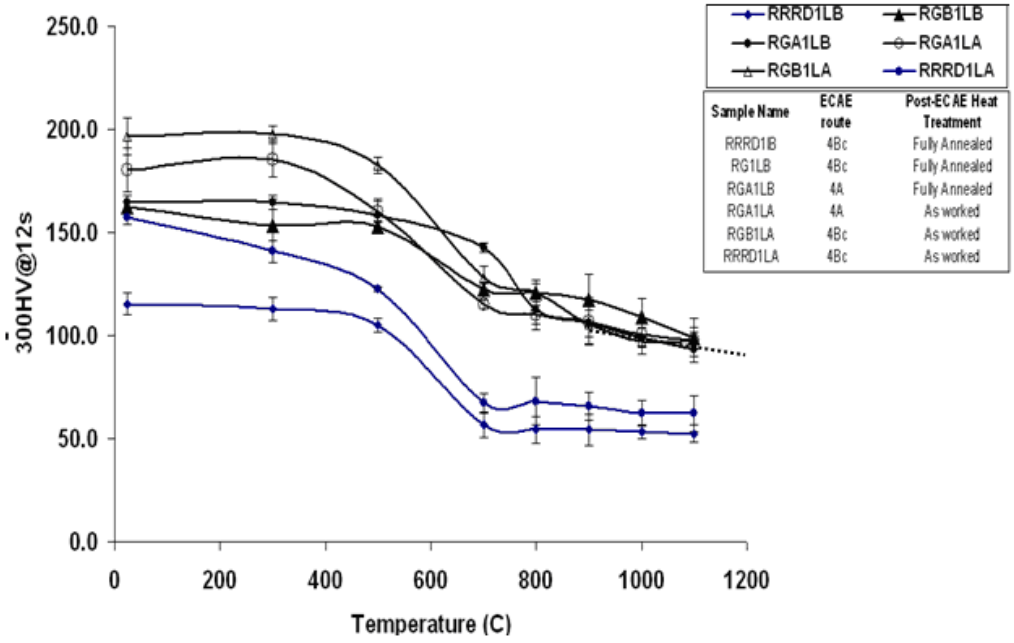

Figure 23. Recrystallization behavior of Nb processed by ECAE routes A and Bc , after cross rolling.

Observations from recrystallization behavior of sheets of lower purity RG material are as follows:

a. Recrystallization curves do not show a sharp drop in hardness.
b. RGB1LA and RGB1LB underwent processing by 4Bc except that RGB1LB underwent an intermediate annealing before rolling. The recrystallization curves seem to follow a similar trend in both cases. The initial hardness of RGB1LA is greater than RGB1LB by a factor of ~50HV, which is consistent with the RRR samples RRRD1LA and RRRD1LB which also underwent similar processing conditions.
c. RGA1LA and RGA1LB processed by ECAE 4A compares the effect of intermediate heat treatments with the route. As indicated in Figure 23 the hardness values are different with the heavily worked material having a higher hardness. However the recrystallization curves do not follow the same trends indicating that the recrystallization behavior is dependent on the intermediate annealing in RG material.
d. Comparison between RGA1LA and RGB1LA show that RGB1LA has a higher starting initial hardness values compared to RGA1LA, this is a consequence of the higher starting initial hardness of ECAE 4Bc (RGB) sample as compared to ECAE 4A (RGA). The recrystallization curves follow similar trends in both these samples.
e. Comparison between RGA1LB and RGB1LB shows the effect of intermediate full anneal on the different routes 4A and 4Bc. The starting hardness of the samples are about the same, however the recrystallization is different in both

these samples, indicated by the curves not following similar trends. For RG samples the recrystallization depends on the ECAE route.

f. Recrystallization temperature cannot be easily determined from the RG curves and seems to be close to ~900^{o}C where the slope of the curve seems to become linear with a moderate downward slope.

Depending on the ECAE route the recrystallization behavior changes. The recrystallization behavior of RG and RRR sheet material is vastly different. However, separately the sheets processed by ECAE route 4Bc seem to follow similar trends in RRR and RG material.

3. Micrographs of Sheet Materials

To fully depict the recrystallization and grain growth behavior in RRR and RG material, representative micrographs are presented in Figure 24(a-e) and Figure 25.As mentioned earlier the recrystallization temperatues are different in RG and RRR materials and so is the grain growth. The grain growth which is closely related to the recrystallization varies depending on a number factors such as route and heat treatment prior to rolling. However, the details are not further explored, the micrographs presented here represent a pictorial view of grain growth in RRR and RG samples.

The grain growth appears to be rapid in RRR samples, with submicron grains appearing at 600^{o}C which rapidly grow by 650^{o}C to grain sizes of 10-20μm. It can be inferred that the recrystallization temperature is around 650-700^{o}C for RRR Nb. By 900^{o}C the grain size is about ~100 μm and increases to about 200-300 μm at 1100^{o}C, also seen are smaller grains of about ~50-100 μm.

The grain growth in RG samples appear to begins at about 900°C and by 1100°C the grain size is about 10-30 µms. Heat treatments over 1100°C were not done as the tube used to heat treat the samples in the furnace was made of quartz and any temperature higher than 1100°C would risk the quartz reaching the glass transition temperature.

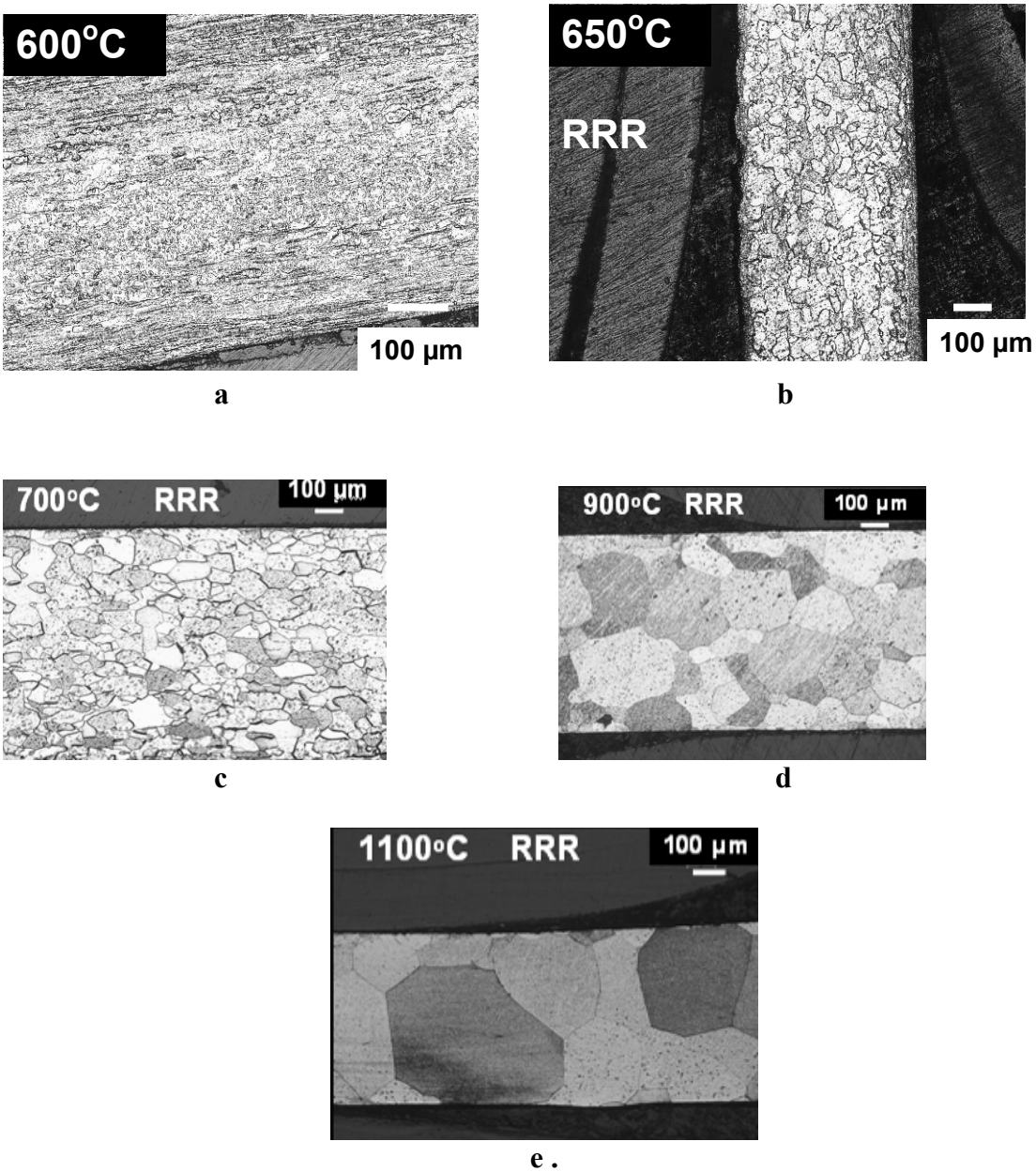

Figure 24(a-e). Optical micrographs of etched RRR Nb showing the grain sizes at various temperatures.

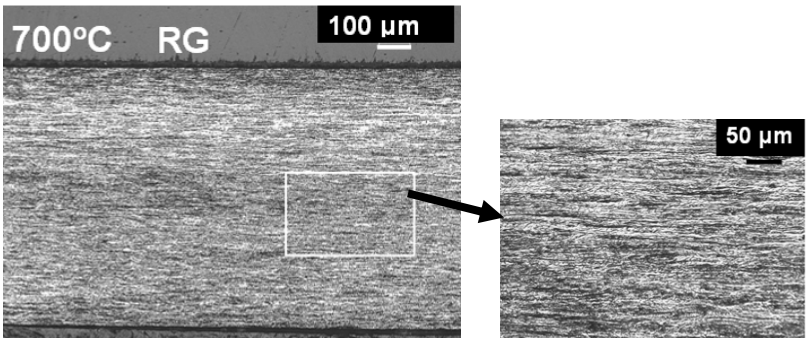

a

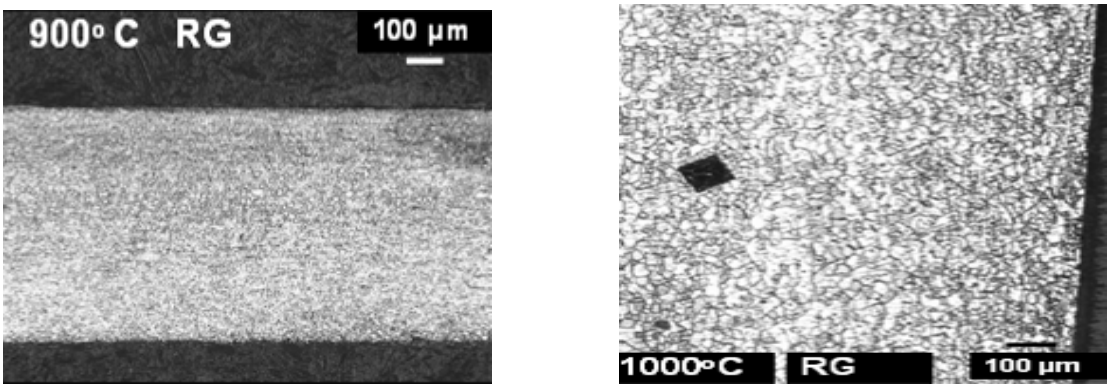

b c

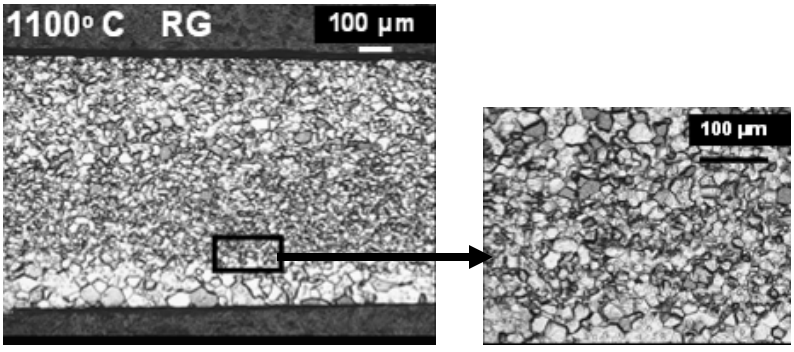

d

Figure 25(a-d). Optical micrographs showing grain sizes at various temperatures in etched RG Nb sheets.

B. Sheet Behavior

To characterize the mechanical properties sheets that were obtained tensile testing was done to determine properties (yield strength, tensile strength, ductility and flow anisotropy) of the sheets along three different orientations namely 0^o, 45^o and 90^o to the final rolling rolling direction. Tensile properties and measurements made during the tensile test, give us an idea about the deformability in the sheets.

1. Tensile Testing of Sheets

The engineering stress strain curves of sheets are presented in Figures 26- 35. There is clear anisotropy in the sheet material which is indicated by the tensile curves The ductility seems to generally be higher in specimens that were oriented at 45^o to the tensile axis. A summary of the tensile test results is presented in Table 11. The key results obtained from these tests in terms of the independent variables are as follows:

a. RRRB2FA and RRRD2FA were repeat samples and as can be seen from their tensile test curves (Figure 26 and Figure 28) and tensile properties in Table 11, it can be inferred that tensile properties are dependent on processing route and reproducible..
b. Samples RRRB2FA, RRRC2FA and RRRA2FA differ only in the ECAE processing route; all the other variables are constant. It can be seen that there is a trend in the yield strength versus orientation depending on the ECAE route. From Figure 36. it is seen that, while 4E and 4A samples show a increasing yield strength value with the angle from the rolling direction 4Bc shows a decrease in the 45 degree orientation. The yield strength values of 4E and 4Bc are

comparatively closer to each other compared to 4A. The anisotropy in the yield strength in the 4A sample with respect to the orientation is far greater in 4E and 4Bc.

c. Comparing samples RRRC2FA and RRRC2FB (from Table 11) we can compare the effect of the post ECAE processing heat treatment. RRRC2FA is a partially annealed sample and shows opposite behavior in terms of the yield strength value to the orientation as compared to RRRC2FB which is an as worked sample.

d. Comparing the RG and RRR samples, the RG samples have much higher yield strength, roughly thrice the strength of the RRR samples. Comparing RGB1LB and RRRD1LB which were both processed similarly, with the only difference being the purity, we see that the trends in the yield strength versus the orientation are similar.

e. The strain hardening exponent of the RRR samples was about 0.26-0.33, except for sample RRRA2FA sample oriented at 90^{o} for which it was 0.19.

f. There is no clear relation between the strain at necking and the independent variables, however the highest strain at necking ~0.3 was seen for RRRA2FA sample in the 0 and 45^{o} orientations.

g. The maximum difference in the strain values with respect to the orientation was seen in RRRB2FA and RRRC2FB. RRRB2FA had a strain at necking as low as 0.17 in the 90^{o} orientation and 0.29 in the 45^{o} orientation. Whereas RRRC2FB measured a strain value of 0.32 in the 45^{o} orientation and a low value of 0.21 and 0.22 in the 0^{o} and 90^{o} orientations respectively.

h. RG samples showed lower ductility than RRR samples with their strain values at necking ranging from 0.17 to 0.26.

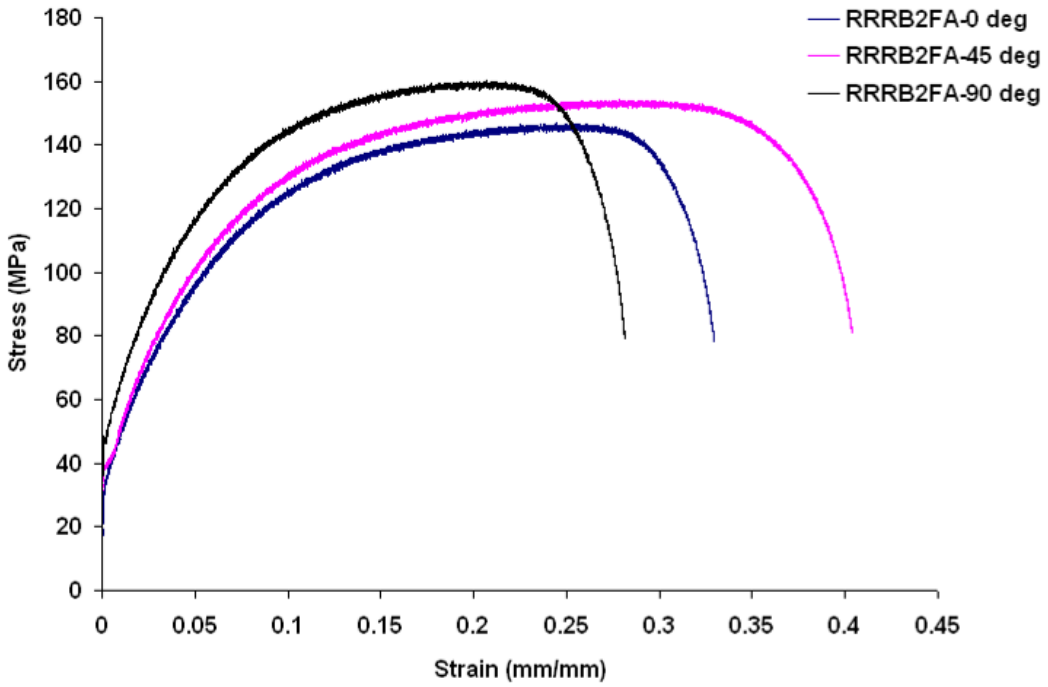

Figure 26. Tensile test curves of sample RRRB2FA.

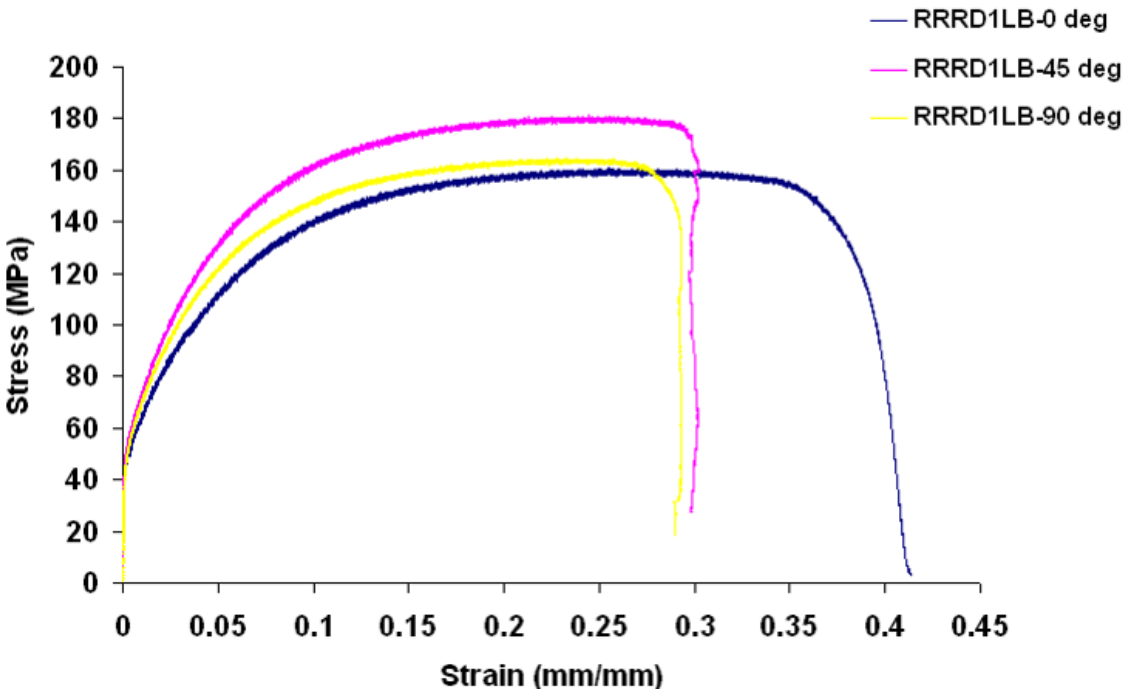

Figure 27. Tensile test curves of sample RRRD1LB.

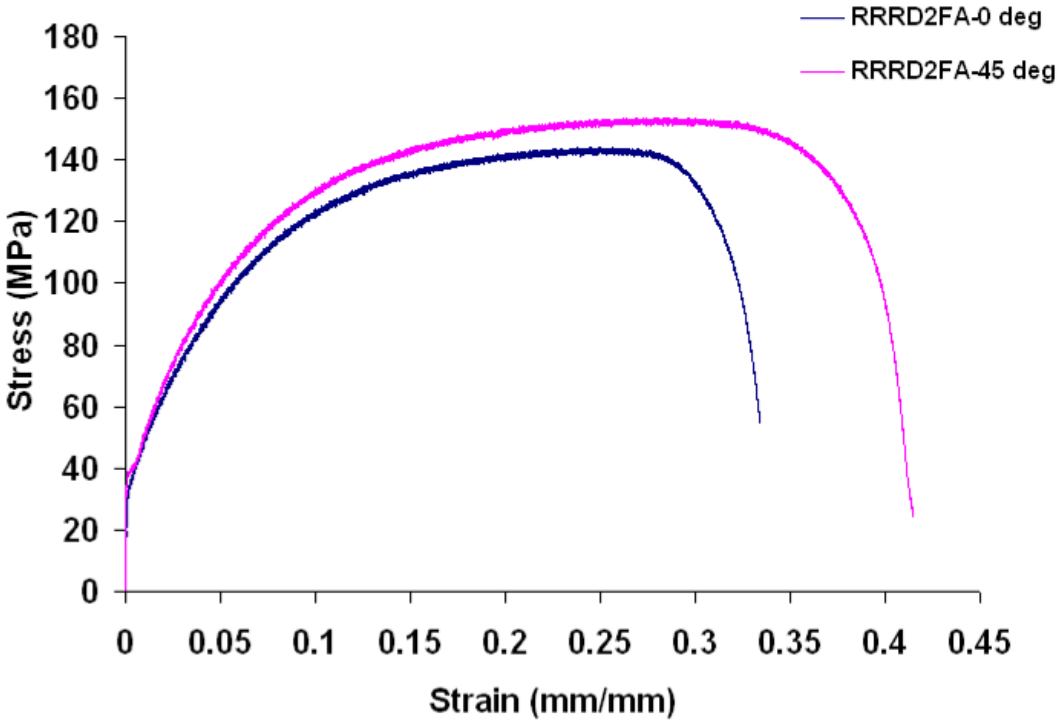

Figure 28. Tensile test curves of sample RRRD2FA.

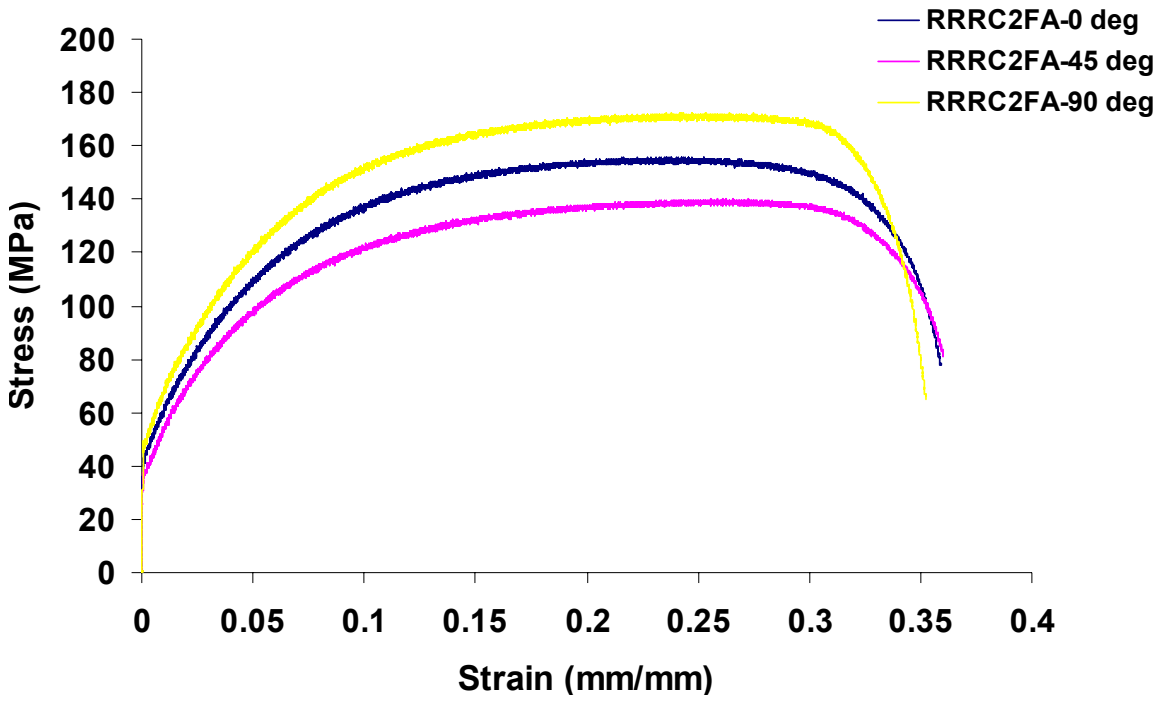

Figure 29. Tensile test curves of sample RRRC2FA.

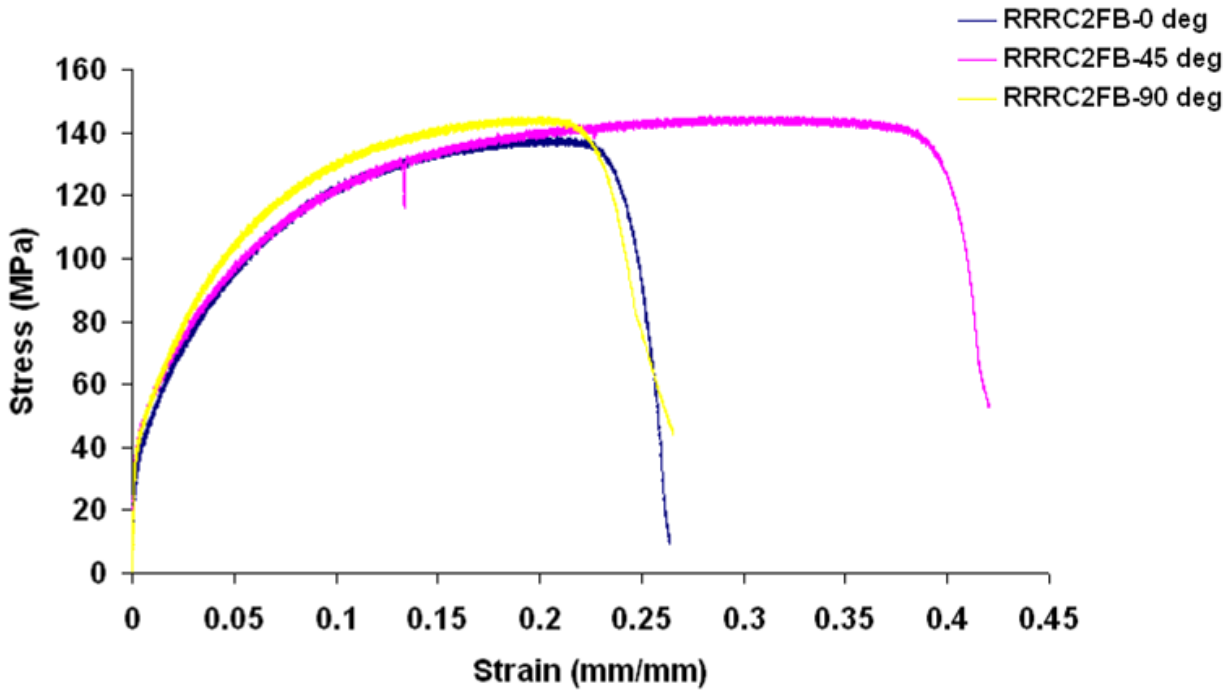

Figure 30. Tensile test curves of sample RRRC2FB.

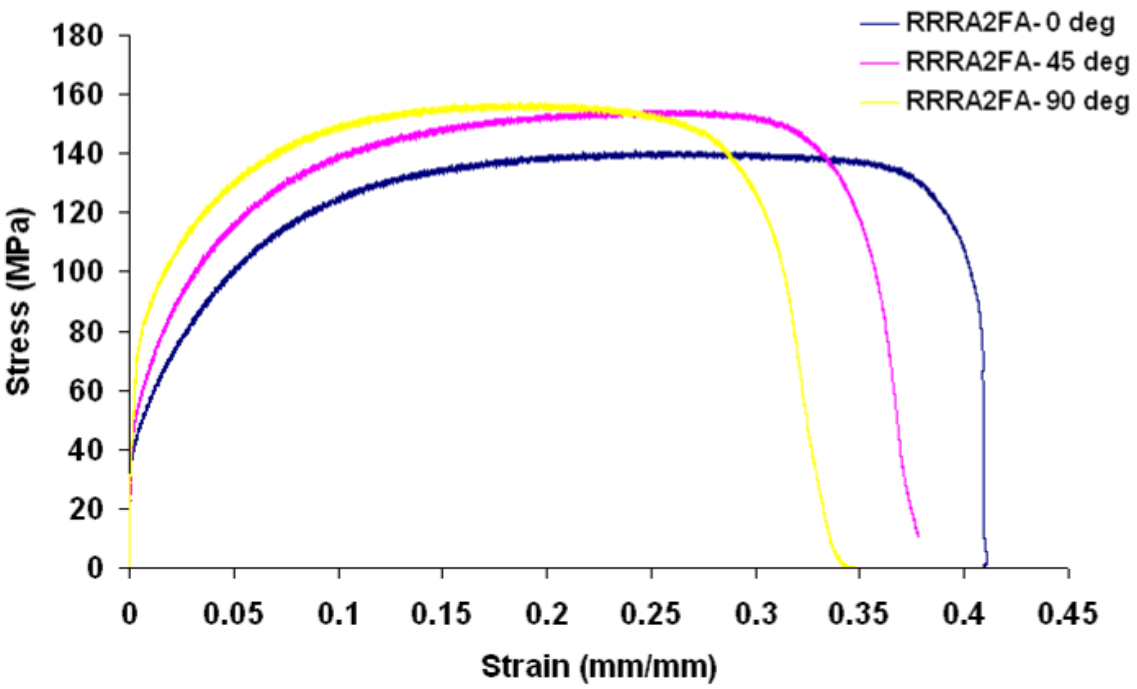

Figure 31. Tensile test curves of sample RRRA2FA.

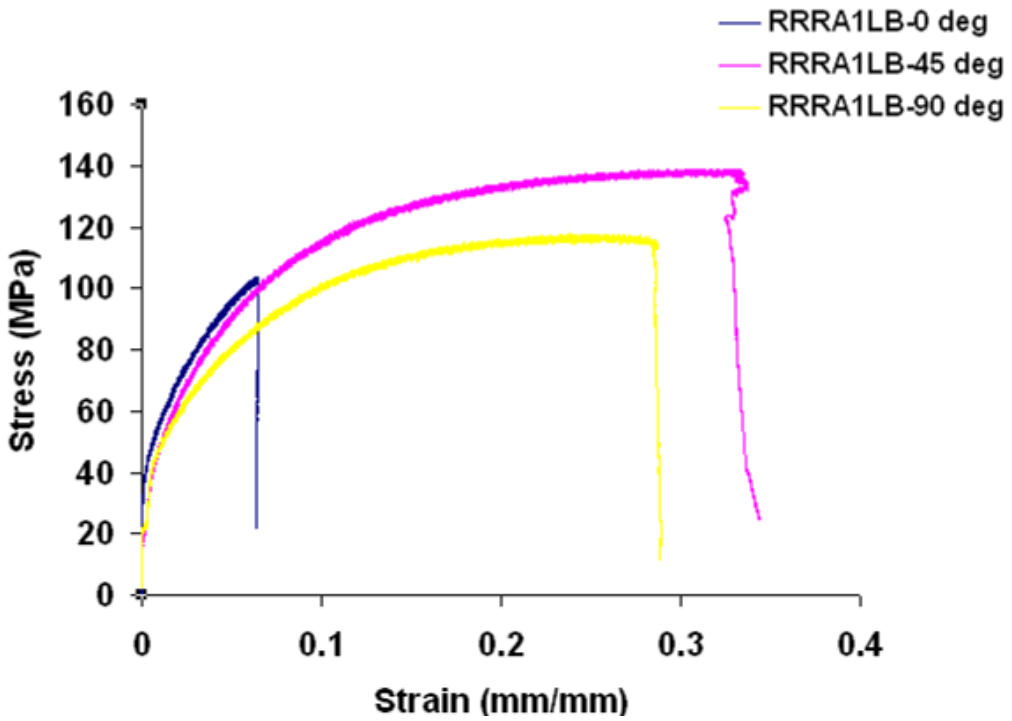

Figure 32.Tensile test curves of sample RRRA1LB.

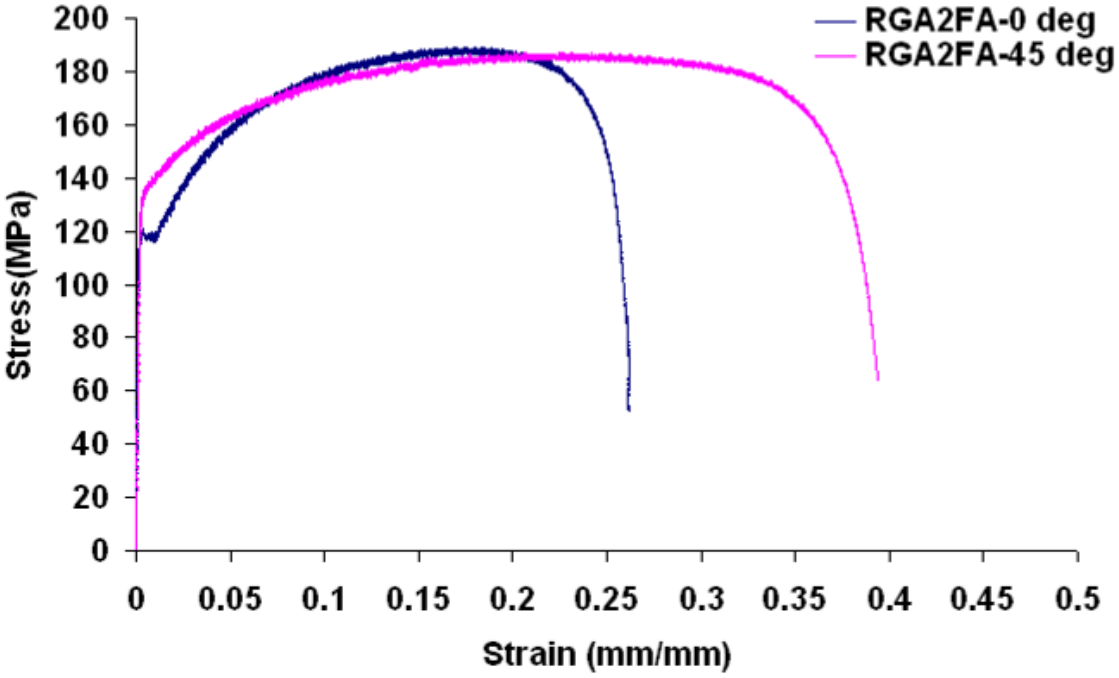

Figure 33. Tensile test curves of sample RGA2FA.

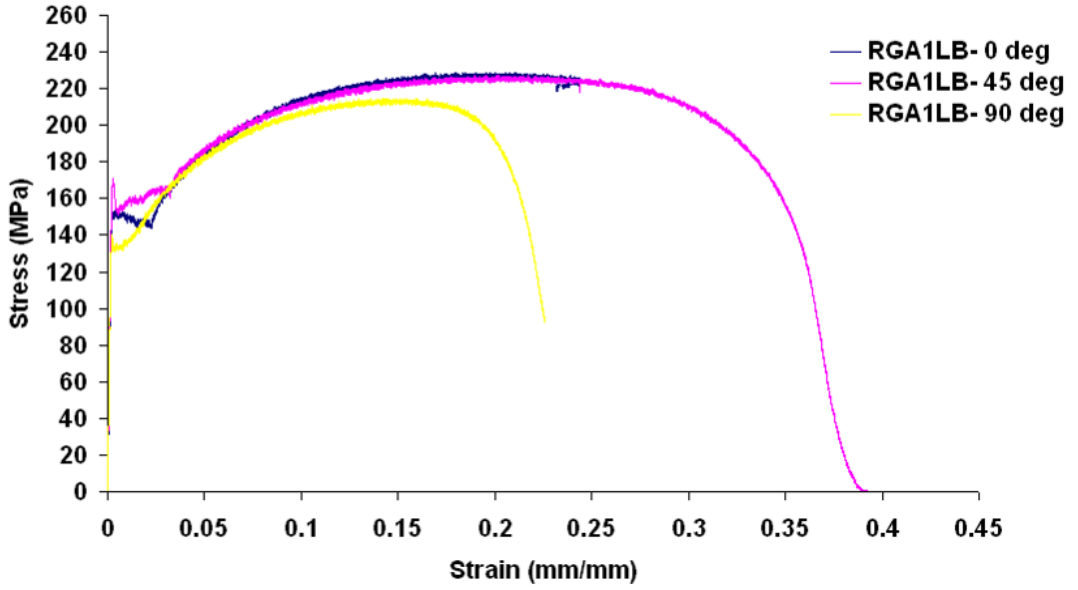

Figure 34. Tensile test curves of sample RGA1LB.

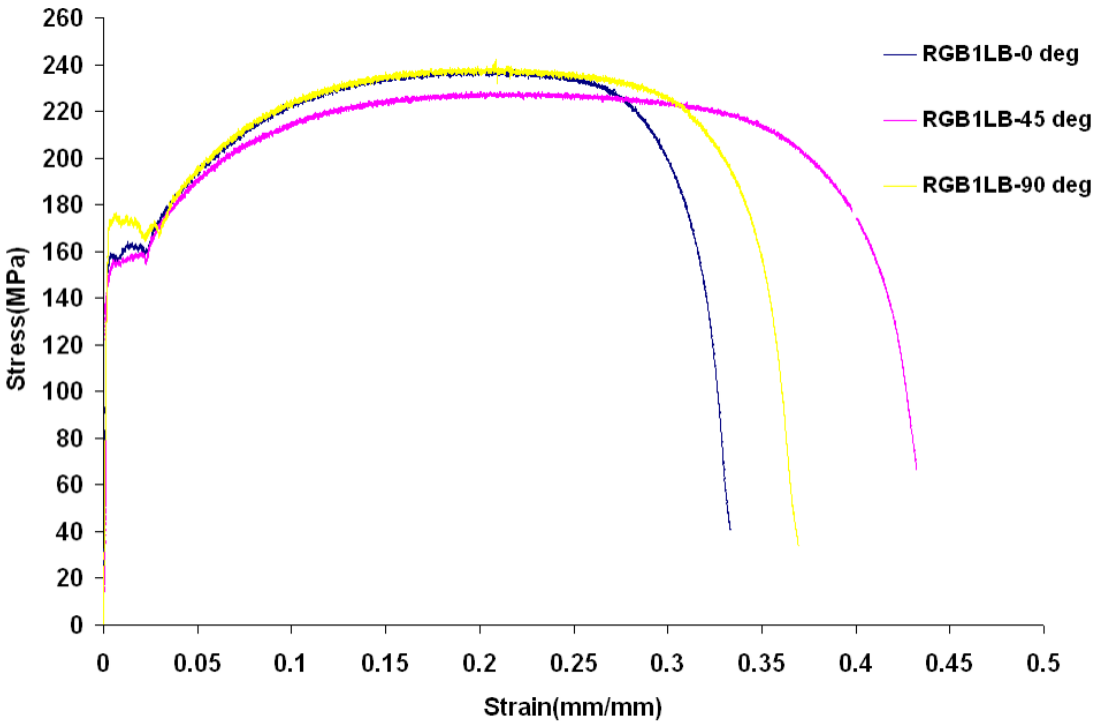

Figure 35.Tensile test curves of sample RGB1LB.

Table 11. Summary of tensile test results.

Sample ID	ECAE route	Post ECAE Heat treatment	Rolling Plane	Sample orientation	Yield Strength (MPa)	Strain Hardening exponent (n)	Strain at necking
RRRB2 FA	4Bc	PA	L	0	36.6	0.31	0.24
				45	40.2	0.31	0.29
				90	49.2	0.28	0.17
RRRD2 FA	4Bc	PA	L	0	36.8	0.33	0.25
				45	39.2	0.32	0.29
RRRC2 FA	4E	PA	L	0	46.0	0.3	0.27
				45	39.7	0.28	0.26
				90	51.7	0.3	0.27
RRRA2 FA	4A	PA	L	0	42.3	0.26	0.3
				45	51.3	0.28	0.26
				90	68.9	0.19	0.24
RRRC2 FB	4E	W	L	0	36.9	0.34	0.21
				45	46.1	0.32	0.32
				90	44.3	0.32	0.22
RRRA1 LB	4A	W	F	0			
				45	22.7	0.3	0.26
				90	21.8	0.31	0.27
RRRD1 LB	4Bc	FA	F	0	50.4	0.27	0.26
				45	57	0.34	0.26

Table 11 Continued

Sample ID	ECAE route	Post ECAE Heat treatment	Rolling Plane	Sample orientation	Yield strength (MPa)	Strain Hardening exponent (n)	Strain at necking
				90	52.4	0.29	0.27
RGA2FA	4A	PA	L	0	121.0		0.2
				45	132.9		0.25
RGA1LB	4A	W	F	0	171.0		0.22
				45	148.5		0.22
				90	154.5		0.17
RGB1LB	4Bc	FA	F	0	150.9		0.2
				45	162.4		0.2
				90	132.4		0.26

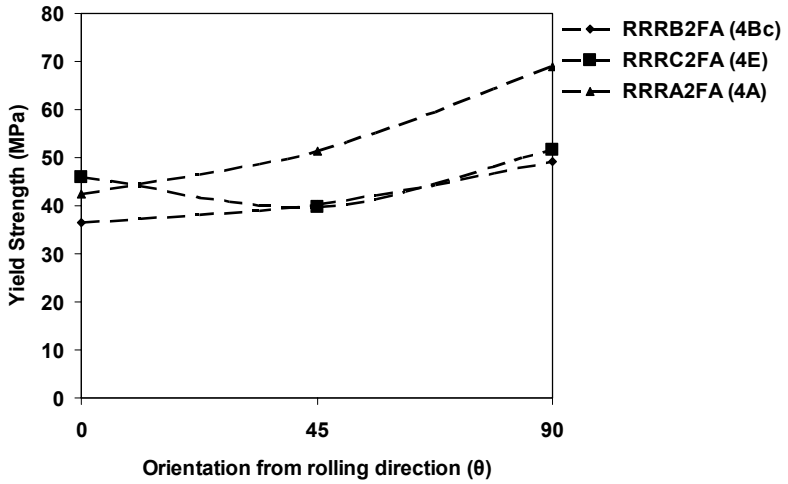

Figure 36. Yield strength versus orientation in RRR annealed sheet for ECAE routes 4A, 4E and 4Bc.

C. Anisotropy in Sheets

Formability is measured in terms of mean plastic strain ratio (r_m) and anisotropy (Δ r). The definitions of these are as mentioned in the literature survey section. Sheets with good formability have high average plastic strain ratios and low anisotropy. Hence a ratio of the anisotropy to the plastic strain ratio could be one way to define to characterize the ductile quality of the sheet. Lower the value of this ratio, better the formability. An ideal ratio is zero with means that there is no anisotropy which translates into better formability. Table 12 presents the calculated plastic strain ratios and anisotropy values of the samples that were tensile tested. A point to be noted here is that comparing the strain values from the uniaxial tensile test may or may not give an exact idea of the formability as the values required for formability are biaxial and hence this measure r_m and Δ r needs to be taken into account. To broadly group samples into two categories it is assumed that $|\Delta r/r_m| > 0.5$ means high anisotropy and $|\Delta r/r_m| < 0.5$ means low anisotropy. Lower anisotropy is what is desired for the application.

From Table 12. we see that there is significant anisotropy in the sheets, a fact already evident by the tensile test curves. Considering the values of $\Delta r/r_m$ we observe that:

a. Among the RRR material high ratios were obtained for samples RRRA2FA and RRRC2FB these were processed by routes 4A partially annealed and cross rolled and 4Bc as worked and cross rolled respectively. Both were rolled with the longitudinal (L) planes brought together. For RRR material Figures 37- 38 show the plots of high and low $\Delta r/r_m$ ratios. A low $\Delta r/r_m$ ratio implies that the Δr values are closer to a straight line as can be seen from Figure 38 for sample RRRD1LB.

b. Among RG material RGB1LB and RGA1LB have high ratios, they were processed by 4A as worked and cross rolled with the flow planes (F) together and 4Bc is fully annealed and rolled with the flow planes together. These high ratios are undesired

c. Considering the samples RRRB2FA (-0.18), RRRC2FA (-0.03) and RRRA2FA (-1.45). All the samples differ only in their ECAE processing and from this we see that 4E is better than 4Bc which is better than 4A for a sample partially annealed and cross rolled.

d. Comparing RRRC2FA (0.03) and RRRC2FB (1.33) we see that for a sample processed by route 4E and cross rolled in L, and as worked gives a much lower anisotropy ratio than a partially annealed material.

e. RRRB2FA (-0.18) and RRRD1LB (-0.29) are both processed by ECAE 4Bc. RRRB2FA was partially annealed and rolled in L whereas RRRD1LB was fully annealed and rolled in F. The anisotropies are somewhat comparable (the difference between them is relatively less) with respect to other pairs excluding RRRB2FA - RRRC2FA pair. This suggests that with route 4Bc the rolling plane or the intermediate heat treatment may not be that critical.

f. The relationship between the ECAE routes, intermediate heat treatments and the planes cross rolled is complicated. More information is required to relate these variables. In order to do so we must look at the texture produced.

Table 12. Plastic strain ratio and anisotropy of sheet.

Sheet ID	r_0	r_{45}	r_{90}	r_m	Δr	$\Delta r/r_m$
RRRB2FA	0.53	1.36	1.76	1.25	-0.22	-0.18
RRRC2FA	0.40	0.72	1.00	0.71	-0.02	-0.03
RGB1LB	0.43	1.13	0.44	0.78	-0.69	-0.89
RRRA1LB	-	1.34	0.07	-	-	-
RRRD2FA	0.21	0.68	-	-	-	-
RGA2FA	1.20	1.86	1.05	1.49	-0.74	-0.50
RGA1LB	2.44	3.33	0.27	2.34	-1.97	-0.84
RRRD1LB	0.42	0.72	0.66	0.63	-0.18	-0.29
RRRA2FA	0.11	0.59	0.08	0.34	-0.50	-1.45
RRRC2FB	1.15	0.19	0.76	0.58	0.77	1.33

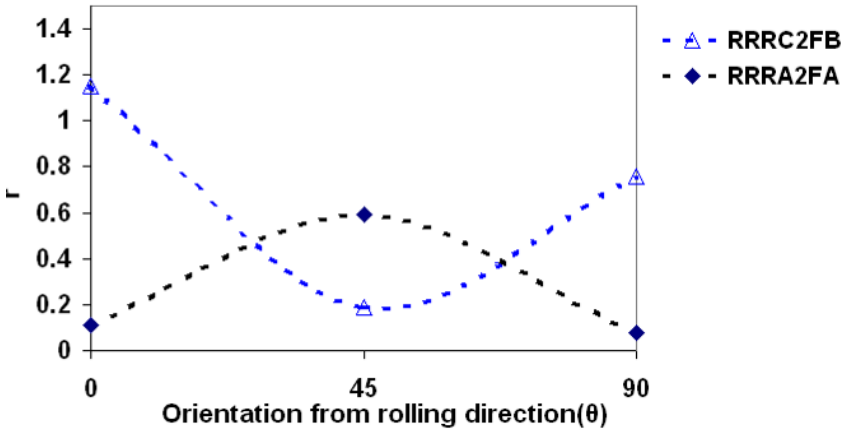

Figure 37. Variation of r with rolling direction, showing samples that have high $\Delta r/r$ ratios.

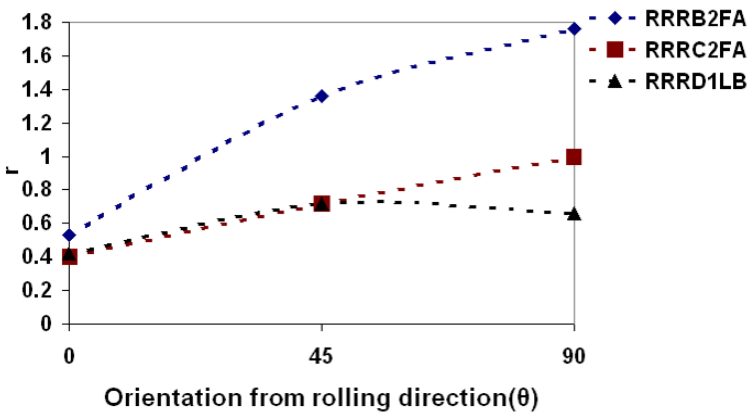

Figure 38. Variation of r with rolling direction, showing samples that have low Δr/r ratios.

D. Texture in Sheets

Formability is closely related to textures that are observed in the sheet material. This makes texture an important component of our analysis. Figure 39 -48 show texture measurements and orientation image maps (OIM's) of the annealed sheet samples. Table 13 summarizes the microstructure of the sample along with the anisotropy ratio obtained.

Presented below are observations that relate the formability behavior with the texture information:

a. Comparsion between the repeat samples RRRB2FA and RRRD2FA as seen in Figure 39 and Figure 40 indicate that the texture obtained in both these samples have only a few similarities, both have a high {100} components also called the rotated cube components which are depicted by the pink colored grains in the texture maps. However, there is a presence of a strong {111} component in RRRB2FA (also called the γ fiber depicted by blue) which is very weak in RRRD2FA.

b. In the repeat samples, the grain sizes are different with RRRB2FA having lesser average grain size and tighter distribution compared to RRRD2FA.

c. From the previous discussion on anisotropy we have samples RRRB2FA(Figure 39), RRRC2FA (Figure 41), RRRD1LB (Figure 43) and RGA2FA (Figure 47) have a low anisotropy ratio. Comparing the texture maps of these samples we see can see that, all these samples have a smooth {111} component, a stronger {110} component (also called the α fiber) and a weaker {100} component .

d. Samples with higher anisotropy ratios namely RRRA2FA(Figure 42), RRRC2FB(Figure 44), RGB1LB(Figure 46) and RGA1LB(Figure 48) have a strong {100}component with the absence or weaker {110} component. In most cases the {111} component is weaker.

e. It appears that lower anisotropy is obtained by specific combinations of the different fiber components {100},{110} and {111} as observed in sample RRRC2FA.

f. For the RRR samples which were partially annealed after ECAE processing and cross rolled in L , it appears that route 4A produces a strong rotated cube component, whereas 4E produces a smooth gamma fiber and a strong alpha fiber. Route 4Bc seems to produce a different results in repeat samples, the common fiber among the two being a weak alpha fiber.

g. To see the effect of impurity content we compare samples RGA1LB and RRRA1LB which were both processed similarly, we find that the RG sample shows the presence of a moderate rotated cube component which is practically

absent in the RRR sample. Also, the RG sample shows a smooth gamma fiber structure, whereas the RRR sample has a punctuated gamma fiber.

h. To see the effect of the rolling plane on a RRR sample processed by 4Bc we can compare the texture obtained in RRRB2FA and RRRD1LB.Rolling the L planes together seems to give to a strong punctuated gamma fiber compared to a predominant strong rotated cube obtained by rolling the F planes together.

i. To compare the effect of the intermediate heat treatment we can compare the samples RRRC2FA and RRRC2FB. Partially annealing the sample seems to produce a smooth gamma fiber and a strong alpha fiber as compared to a strong split rotated cube obtained in a sample that was rolled as worked.

j. To see the effect of the route in low purity RG samples we can compare RGB1LB and RGA1LB. The difference between the sample processed by Route Bc is primarily that it produces more rotated cube components than the sample processed by Route A. Both these samples were rolled in F.

k. Textures produced are dependent on the route, rolling plane, intermediate heat treatment and also the purity of the sample.

l. Purity affects the texture and hence RG and RRR samples do not produce the same sort of texture even if processed by similar processing techniques.

Table 13. Summary of microstructure obtained in sheets.

Sample Id	Purity	Processing[+]	Microstructure		$\Delta r/r_m$
			Texture	Grain size (μm)	
RRRB2FA	High	4Bc+PA+L	Strong punctuated γ, moderate α , weak split rotated cube	30-40	-0.18
RRRC2FA	High	4E+PA+L	Smooth γ, strong α and a weak split rotated cube	20-40	-0.03
RGB1LB	Low	4Bc+W+F	Smooth γ, strong split rotated cube.	20-70	-0.89
RRRA1LB	High	4A+W+ F	Strong punctuated γ, moderate α	10-40	-
RRRD2FA	High	4Bc+PA+L	Strong rotated cube, weak α	15-60	-
RGA2FA	Low	4A+PA+L	Strong split rotated cube, moderate α, γ	10-30	-0.50
RGA1LB	Low	4A+W+F	Smooth γ, moderate rotated cube	10- 40	-0.84
RRRD1LB	High	4Bc+FA+F	Strong split rotated cube, weak α, γ	10-50	-0.29
RRRA2FA	High	4A+PA+L	Strong split rotated cube	20-120	-1.45
RRRC2FB	High	4E+W+L	Strong split rotated cube, weak α	30-90	1.33

+ The processing is mentioned in the following order ECAE route + Heat Treatment + Cross rolling Plane.

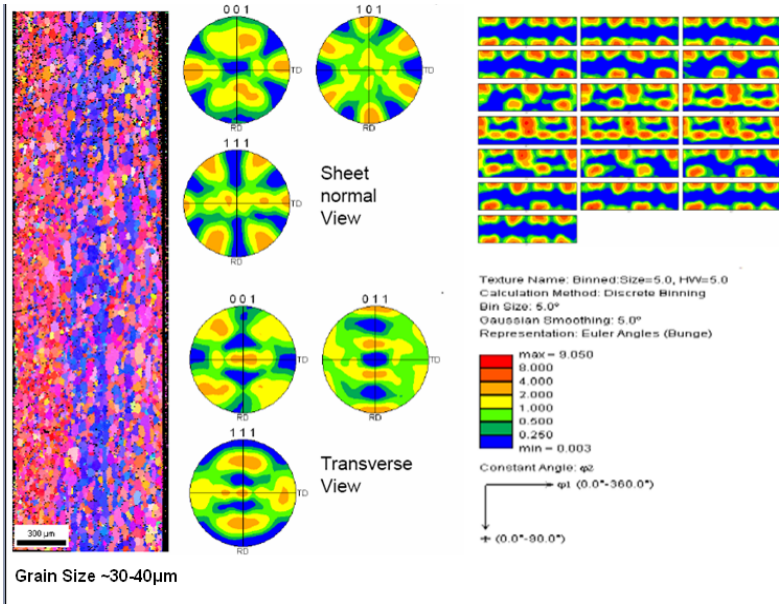

Figure 39. Texture map and OIM of sample RRRB2FA.

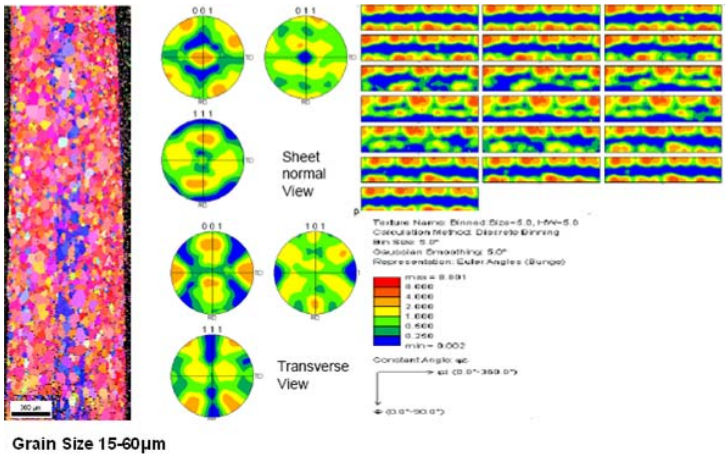

Figure 40. Texture map and OIM of sample RRRD2FA.

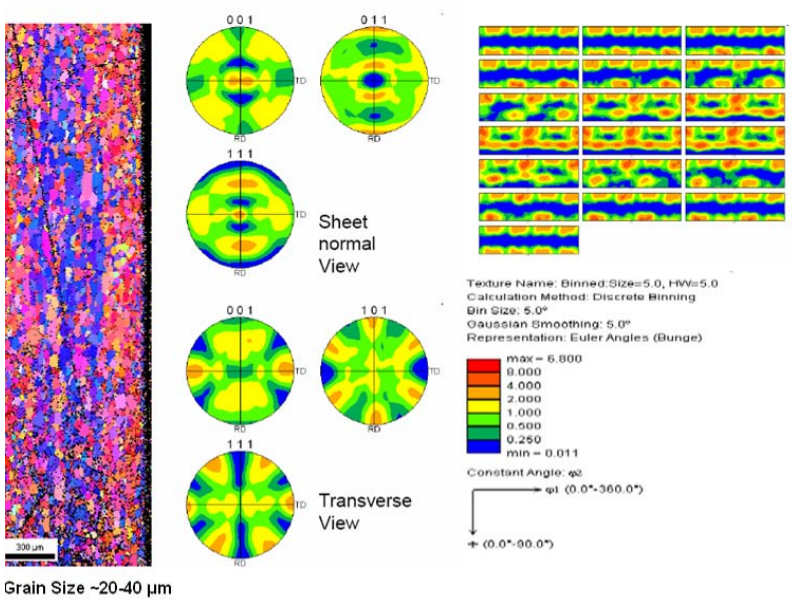

Figure 41. Texture map and OIM of sample RRRC2FA.

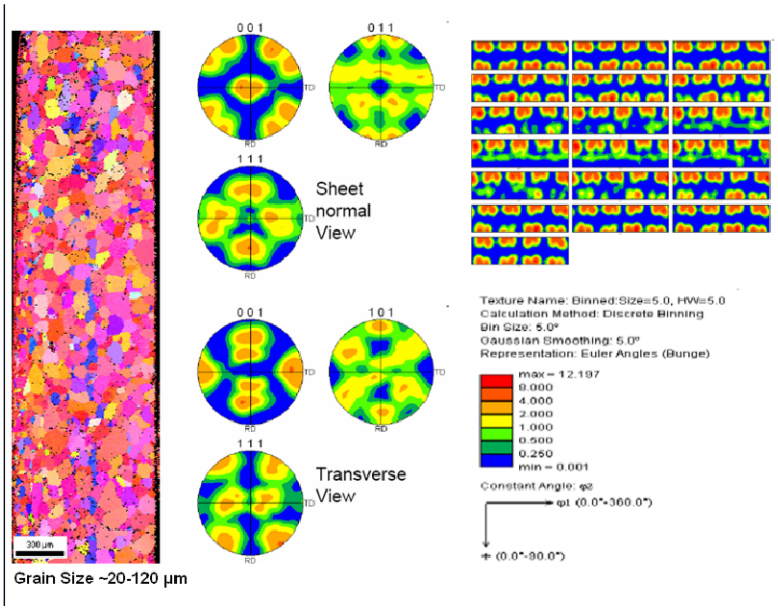

Figure 42. Texture map and OIM of sample RRRA2FA.

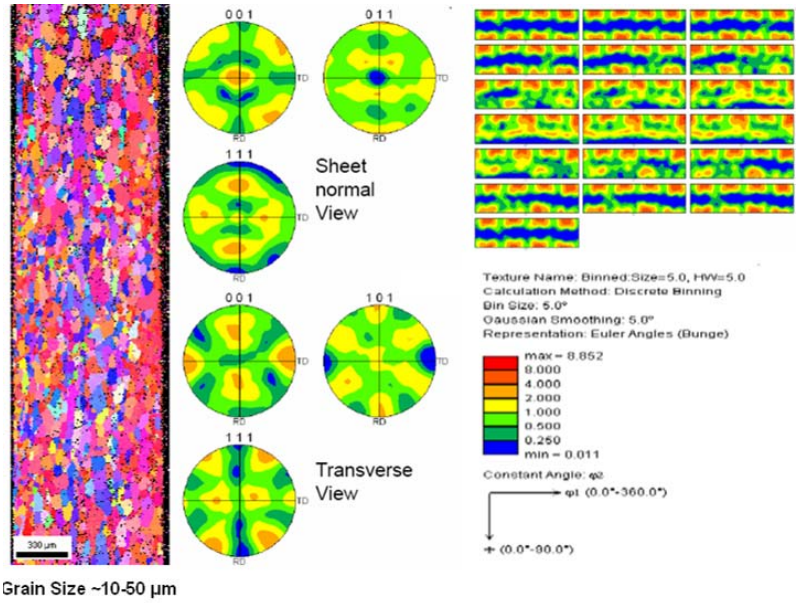

Figure 43. Texture map and OIM of sample RRRD1LB.

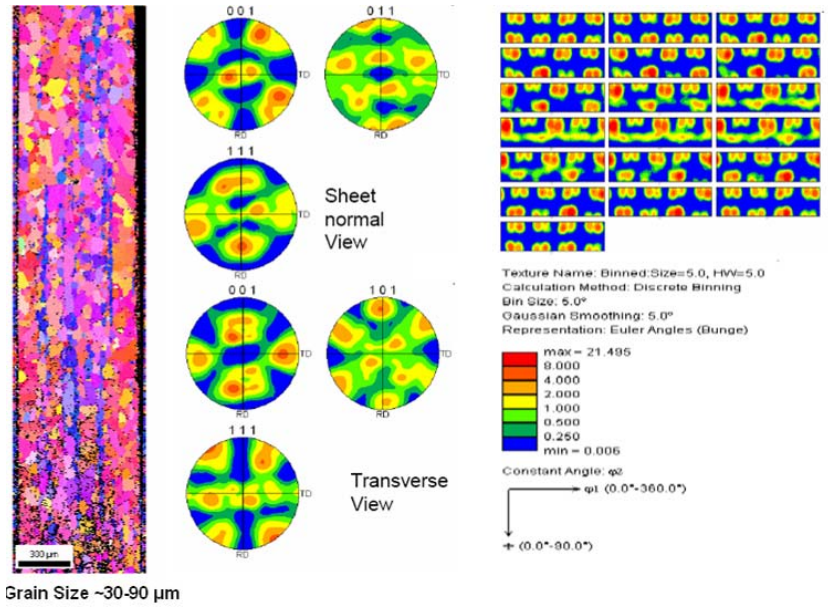

Figure 44. Texture map and OIM of sample RRRC2FB.

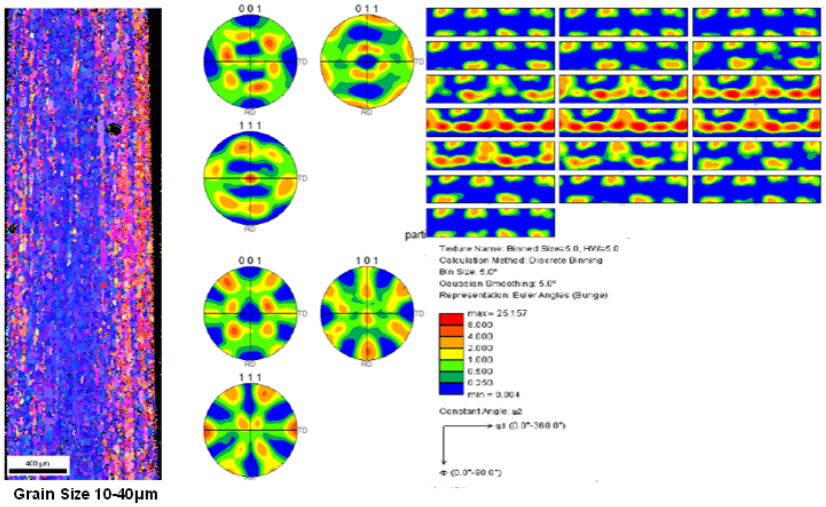

Figure 45. Texture map and OIM of sample RRRA1LB.

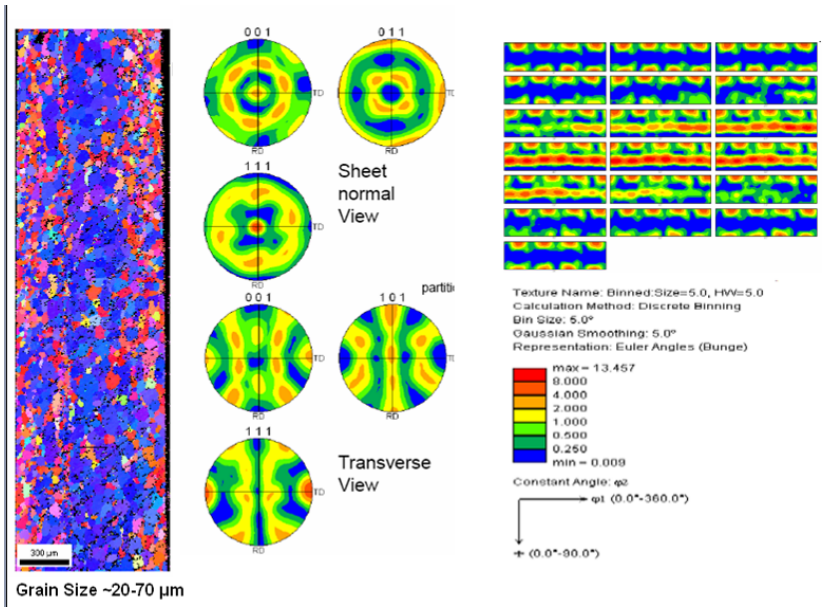

Figure 46. Texture map and OIM of sample RGB1LB.

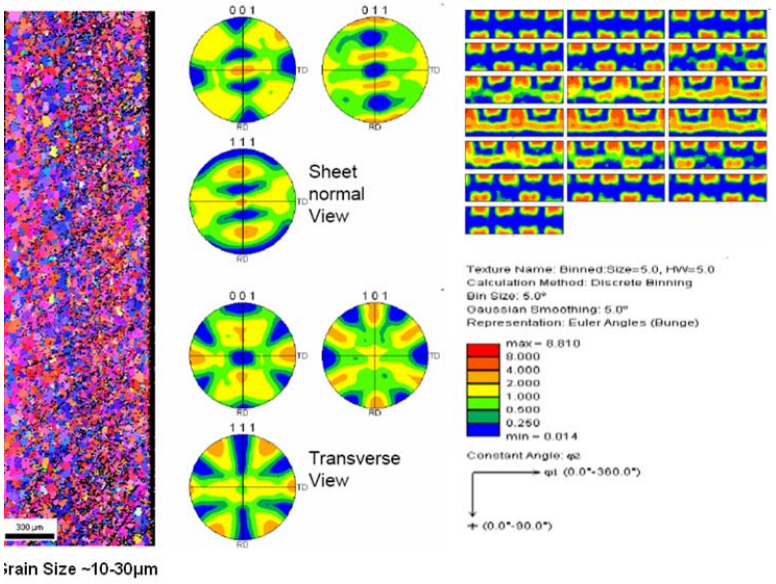

Figure 47. Texture map and OIM of sample RGA2FA.

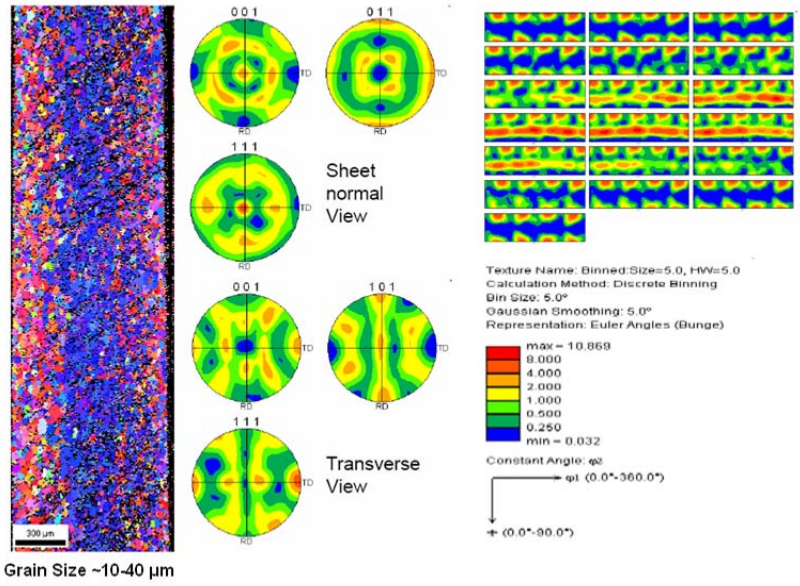

Figure 48. Texture map and OIM of sample RGA1LB.

CHAPTER V

DISCUSSION

A. Recrystallization Behavior

Recovery of deformed grains precedes recrystallization. Complete recovery of grains rarely occurs in materials that have undergone large deformations and usually recrystallization processes occur well before complete recovery [18]. In this section we discuss the observed results of the recrystallization curves plotted for the bulk samples and rolled sheet samples.

1. ECAE Processed Billets

From the recrystallization curves presented in the previous section (Figure 49.), the purity of the sample has a significant influence on the recrystallization behavior. Table 14 shows the dramatic effect of the purity on the recrystallization temperature in commercial purity and zone refined metals[18]. The major impurity between RG and RRR samples is Ta, which is present as a substitutional impurity. The effect of small levels of impurity directly affects the grain mobility and migration, usually lowering it. This means that for the recrystallization and subsequent grain growth mechanisms to be operable more energy is required which translates to a higher temperature. This is why there is an increased recrystallization temperature in RG material compared to RRR material.

Table 14. The effect of purity on the temperature of recrystallization for several commercial metals (taken from Dimitrov et al. 1978) [18].

Metal	**Recrystallization Temperature in ^{o}C**	
	Commercial Purity	**Zone Refined**
Aluminium	200	-50
Copper	180	80
Iron	480	300
Nickel	600	300
Zirconium	450	170

It is also seen that the recrystallization temperature is also varied depending on the ECAE route. It is seen that the strain path has an influence on the recrystallization behavior. Experiments by Embury et al. [60] suggest that the strain path reversals lead to a higher recrystallization temperature. However, comparing the two ECAE routes 4A v/s 4Bc, a 90^{o} rotation about the axis is supposed to introduce complex strain paths and destabilize the distorted grains leading to higher angle grain boundaries and hence a lower recrystallization temperature [61]. However our observation has been contrary to this, to fully understand the recrystallization behavior depending on the route a thorough analysis on the sub structure growth and recovery processes needs to be done.

2. Rolled Sheets

There is a drop in the recrystallization temperature between the as ECAE processed samples and ECAE processed and rolled samples which can be explained based on the increase in stored energy in the material which is associated with the increase in the number of dislocations and formation of other defect structures such as high dislocation density cell walls, deformation band and shear band regions. These mean a greater driving force for recrystallization and hence the lower recrystallization temperature.

RRR samples show an expected behavior with the hardness leveling off after recrystallization.

RG samples show a recrystallization behavior that is characteristic of discontinuous recrystallization [18], explanation of this behavior in these samples can be complicated :

a. The strains received was extremely large and long scale heterogeneities would play an important role in recrystallization.
b. The evolution of texture in the sample, or heterogeneity of texture produced during the processing stage will tremendously affect the recrystallization of different grains., seen in Figure 49 which shows the proposed dependence of the different orientations on the nucleation and hence recrystallization behavior for IF steel based on the experiments done on annealing behavior of cold rolled IF steel to various reduction ratios [62].
c. Also, though the texture produced are the same for certain samples the strain path history seems to effect the recrystallization behavior of the sample significantly. So a sample with the same texture prior to recrystallization would show a significantly different behavior if the strain paths are different.

Clearly, this is applicable to our sample as not only are the routes different, the planes that are rolled are different too.

A complete analysis of the recrystallization behavior would have to take into account the following variables: deformation microstructure, strain paths, sub structure produced and recovery processes. Future work on this is needed.

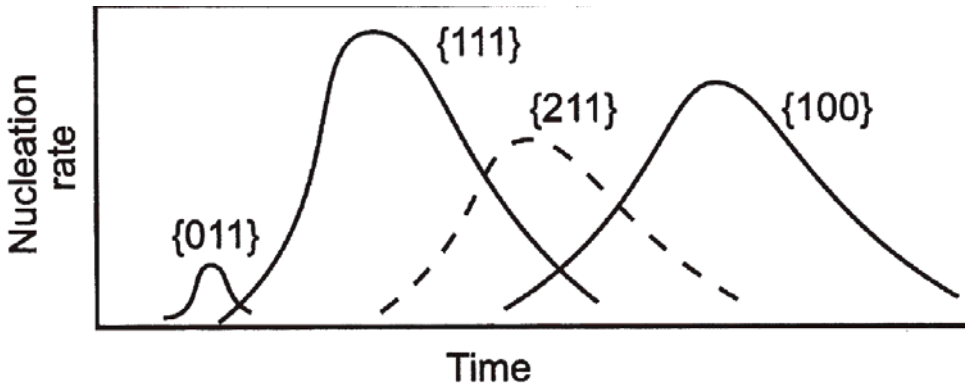

Figure 49. Schematic representation of the orientational dependence of nucleation in deformed iron. [62]

B. Sheet Behavior

The clear anisotropy in the sheets can be attributed to the directionality produced by rolling. Though the samples have been cross rolled there is certain directionality. To achieve anisotropy, the sample probably needs to be rotated by a sample angle after every rolling pass.

The high ductility observed in the 45^o direction to the rolling direction can be attributed to lower flow stresses in the 45^o direction as compared to 0^o and 90^o. This result is consistent with that obtained by Roberts in the analysis of forming of Cu sheets with cube textures [63].

Comparing the different purity levels, we can see that RG samples have a higher yield stress compared to RRR samples. The higher yield strength is attributed to presence of Ta, this is observed in other literature [10,16]. This increased yield strength is an effect of the lattice strains introduced by the impurity atom Ta in our case. The stain field interactions of the impurity atoms hinder the movement of dislocations by diffusing and segregating around the dislocations which reduces the overall energy of the system [10]. Yield behavior is also typically related to grain size by the Hall-Petch equation which states that the yield strength is inversely proportional to the square root of the grain diameter (d). This assumes anisotropy of the material behavior, however the sheet samples under consideration are isotropic and textured. The Hall- Petch equation is not valid for these results. There seems to be no apparent trend in the yield behavior. To obtain further understanding about yielding, the yield strength must be analyzed with respect to specific textures for these sheets.

The yield strength values obtained are comparatively lower than those in literature [10], the difference in yield strengths maybe due to thin specimens (0.5-0.8 mm thick) used in our study. With such thin specimens there are size effects observed which lead to slight differences in yield strength values [64]. It would hence be ideal to compare the yield values of specimens with similar thickness, especially when they are less than a millimeter. The reason for such a deviation has been attributed to reduced constraint on the grains due to the free surface. In thin specimens, the percentage of grains exposed to free surface is much more than that in a thicker sample. Reduced constraints on these grains lead to yielding at much lower flow stresses [64, 65]. Figure 50 shows the study

conducted by Rauela.et al. on CuZn15 tensile specimens, with an estimated average grain size of 25μm.

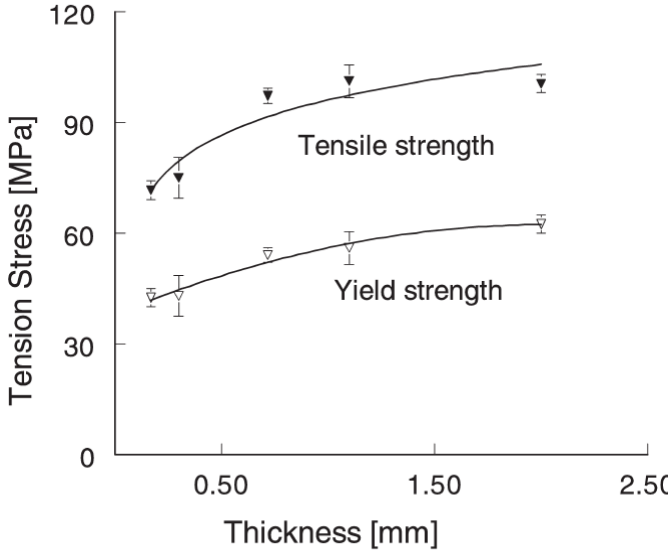

Figure 50. Variation in yield strength versus thickness in CuZn15 alloy with an average grain size of 25μm [64].

C. Texture in Sheets and Formability

The variety of textures is observed are in Nb sheets made by preprocessing bulk Nb by ECAE. The textures primarily observed in our study are strong gamma fiber, strong rotated cube and strong alpha fibers or a combination of these fibers in different ratios. Among these, the gamma fiber {111} texture is the most preferred for forming operations [3] , as suggested by Wilson's work on Cu sheets. However, in our study we see that a combination of gamma fiber and alpha fiber gives the lowest anisotropy ratio, suggesting that sheet anisotropy behavior in b.c.c and f.c.c metals may be different.

Previous literature suggests that gamma fiber(blue) textures are intensified after high rolling reductions and during annealing of these sheets [20,21]. One important observation from the work of Vandermeer is that the textures obtained in cold rolled Nb is that the texture components are diffuse, compared to the strong textures obtained by this study. This maybe due to the strong tendency of Nb to form shear bands, which can lead to intense local rotations leading to inconsistent textures in conventional processing. We do not expect shear banding in routes such as A, as compared to Bc and this could play an important role in obtaining repeatable textures in sheets in the absence of shear banding. With proper ECAE processing the tendency of forming shear band maybe reduced. The gamma fiber texture {111} is considered to be the most preferred orientation for growth and the recrystallization behavior and is explained mostly in terms of lower elastic modulus or lower stored energy in these configurations [66]. However, this theory cannot completely explain the textures obtained in the present study.

The evolution of recrystallization textures is dependent on other factors involving [18]:

a. Effect of strain and strain path.
b. Orientational growth that takes place after recrystallization.
c. Starting textures
d. Purity of the sample.

Any model that could be used for texture development of this study must address these issues as well. The most important among these being the effect of strain and strain path, which is most predominant effect as suggested in this study.

Texture evolution in repeat samples appear to be different, this is particularly surprising. One way to confirm this result is to analyze different samples from various parts of the

sheets and look at the texture developed. Our results of texture, are more macroscopic than that from TEM samples. However we do not know if there is any variation across the width of the sheet. Texture evolution in rolled sheets depends on a number of rolling parameters, which may have a influence on our study such as:

a. Reduction per pass- Higher the reduction per pass, more uniform is the texture evolution. Our reduction per pass was 10-20% which is high and hence we expect to have considerable uniformity.
b. Total reduction – Heavily worked material i.e. with rolling reduction greater than 80% has a considerably different texture than that of lightly rolled materials. As the thickness of the material is reduced considerably, double shear can occur on the surface of the sheets, leading to a different texture evolution. Our final sheet thicknesses were about 0.5-0.8mm, and there may be this effect of double shear taking place. We might have different results if our final sheet thicknesses were 2-5 mm, even though all the processing were the same.
c. Initial microstructure – Initial microstructure seems to play a very important role during rolling. There is a critical grain size above which we can expect deformation banding to take place, which will give rise to differences in recovery phenomenon. Our starting grain sizes were about 10-15 μm and we do not expect deformation banding to take place. However we cannot rule out the possibility of the occurrence of shear bands and long scale microstructure heterogeneities.
d. Friction – Friction during rolling causes heterogenities in texture evolution, well lubricated surfaces seem to have a better homogeneity in rolled sheets.

CHAPTER VI

CONCLUSIONS AND FUTURE WORK

A. Conclusions

1. RG and RRR material shows different recrystallization behavior and different mechanical properties and hence they cannot be used as substitutes for each other in recrystallization experiments.
2. ECAE processed bulk Nb subsequently rolled into sheets shows reproducibility in mechanical properties, but inconsistencies in the textures that evolve.
3. There is significant anisotropy in tensile properties that is observed even in cross rolled Nb samples. Reducing the anisotropy requires a combination of suitable textures namely the gamma and alpha fibers in the final sheet material.
4. The experiments showed that it is possible to obtain some microstructural control after heavy working in extremely pure materials. We were able to obtain a sheet with very low anisotropy of $\Delta r = 0.02$.
5. ECAE combined with rolling may provides a way to control texture in Nb sheet material. Depending on the ECAE route chosen and the planes rolled, a variety of textures were obtained. The texture combinations observed were : a). a strong gamma fiber. b). a strong rotated cube c). strong alpha fiber and d.) different combinations of the fiber textures with various intensities.

B. Future Work

To fully understand the evolution of microstructure in Nb , a comprehensive study of the deformation mechanisms need to done. This involves a thorough study of the

microstructure evolution involving tracking microstructural evolution during ECAE and then during rolling. TEM, in combination with EBSD needs to adopted to track microscopic effects and consider short range effects and macroscopic long range deformation gradients and heterogeneities.

Recovery processes need to further studied with the help of a DSC, as the effects on the physical properties (hardness) are hardly noticed during the recovery stage. Recovery constitutes an important part of the microstructure evolution and needs to be studied in detail.

A channel die experiment is suggested to see if similar textures could be obtained by applying the same modes of deformation as done by specific ECAE routes.

The results that were obtained here seem to be different from those discussed in available literature on bcc metals and hence needs to be verified to establish the repeatability of the results.

Future work could involve modeling the microstructural evolution in bcc metals processed by ECAE in general and Nb in particular.

REFERENCES

[1]. R.Orsund and O.Lohne. Mater Sci Forum.,94 (1992) 753.

[2]. S.Kalpakjian. Manufacturing Processes for Engineering Materials, Addison Wesley, Reading, Massachusetts, 1985

[3]. D.V. Wilson and R. D. Butler. J. Inst. Met., 90 (1961-2) 473-483.

[4]. I. L. Dilamore and W.T. Roberts. Met.Rev., 10 (1965) 271.

[5]. V.M.Segal, Mater.Sci.Eng.A, 197 (1995) 157.

[6]. Ferrasse. S, Segal. V.M, Kalidindi. S.R, F. Alford Mater.Sci.Eng.A, 368 (2004) 28

[7]. Venetsky. S.I, Tales about Metals, Mir, Moscow,1978(English ed by Kittel N.G, 1981).

[8]. Lambert. J.B, Droegkamp.P, in High Temperature Materials and Metals Handbook, 9th ed, Vol.7, ASM International, Materials Park, OH (1984) 764-772.

[9]. John F. P, U.S. Geological Survey, Mineral Commodity Summaries, January 2008, pps 116-117, Accessed: May 25, 2008. from the World Wide Web: http://minerals.usgs.gov/minerals/pubs/commodity/niobium/mcs-2008-niobi.pdf.

[10]. C.K.Gupta and S.K.Puri, Extractive Metallurgy of Nb, CRC, BARC,Mumbai,India 1994.

[11]. Tantalum-Niobium International Study Center website: Accessed on April 10 2008 from the World Wide Web: http://www.tanb.org/niobium1.html

[12]. P. Kumar, J. Less Common Metals, 139 (1988) 149-158.

[13]. E. Fromm, E. Gebhardt , Gase und Kohlenstoff, Metallen., Springer, Berlin (1976).

[14].H.Umezawa, in Single Crystal – Large Grain Nb Technology: International Niobium Workshop, AIP Conf. Proc. 927 (2007) 186

[15].Graham. R.A, in Single Crystal – Large Grain Nb Technology: International Niobium Workshop, AIP Conf. Proc. 927 (2007) 191

[16].R. Grill., A. Gnadenberger , Int J Refract Met H. 24 (2005) 275

[17] G.E.Dieter., Mechanical Metallurgy, McGraw Hill, New York,1986.

[18]. F.J.Humphreys and M.Hartherley, Recrystallization and Related Annealing Phenomena, Elsevier Science, New York,2002

[19]. H.R. Wenk and P. Van Houtte, Rep Prog Phys. 67 (2004) 1367.

[20]. R.A.Vandermeer and J.C.Ogle, Trans. Met. Soc. AIME. 242 (1968) 1317- 1326

[21]. R.A.Vandermeer and J.C.Ogle, Trans. Met. Soc. AIME. 245 (1968) 1511-1518

[22]. H. Jiang , T.R. Bieler, , C. Compton, T. Grimm, Physica C. 441 (2006) 118-121

[23]. H. Jiang, T.R. Bieler, C. Compton, T. Grimm, TMS Letters.1 (2004) 79.

[24]. H. Jiang, T.R. Bieler, C. Compton and T.L. Grimm, in: Proceedings of the Particle Accelerator Conference, Portland, Oregon, IEEE (2003) 1359-61.

[25]. H.R.Z. Sandim , J.F.C. Lins , A.L. Pinto and A.F. Padilha, Mat. Sci. Eng. A. 354 (2003) 217-228.

[26]. H.R.Z. Sandim, J.F.C, Lins, A.L. Pinto, A.F. Padilha, Mater. Sci..Forum. 408-4 (2002) 517

[27]. H.Padamsee, Annu.Rev.Nucl.Part.Sci. 43 (1993) 635-686.

[28]. Superconducting RF Cavities a Primer, Cornell Electron Storage Ring (CESR) website. Accessed on April 5 2008 from the World Wide Web: http://www.lns.cornell.edu/public/CESR/SRF/BasicSRF/SRFBas1.html

[29].International Linear Collider Website.Accessed on April 5 2008 from the World Wide Web: http://www.linearcollider.org/cms/?pid=1000000

[30].G. R. Myneni. Physical and Mechanical Properties of Single- and Large-Crystal High-RRR Niobium, in Proceedings of 12th International Workshop on RF Superconductivity (SRF 2005), July 10-15, Ithaca,New York, USA. Thomas Jefferson National Accelerator Facility Website. Accessed on April 10 2008 from the World Wide Web: http://srf.jlab.org/SingleCrystalNb/pdfs/04%20Myneni%20SCNB%20Brazil.pdf

[31].W. Singer, AIP Conf. Proc. 51 (2006) 837.

[32]. V. Palmieri, in: Proceedings of LINAC98, IL, Chicago, NAL (1998) 697-700.

[33]. P.Kniesel, Nucl Instrum Meth A. 557 (2006) 250-258

[34]. W.Singer, Physica C 441 (2006) 89–94.

[35]. M. Pekeler, in: Proc.of PAC'99, New York, USA (1999) 245-249.

[36]. V. Palmieri, IEEE.T.Appl.Supercon. 9 (1999) 1036-1038

[37]. T. Ota, S. Sukenobu, Y. Tanabe, K. Takaishi, M.Yamada et al.,in: Proceedings of the 8th Workshop on RF Superconductivity, Abano, Italy, ANL (1997) 254-260.

[38]. I. Gonin, I. Jelezov, H. Kaiser, T. Khabibuline, P. Kneisel et al, in: F. Krawczyk,(Eds.), Proceedings of the 9th Workshop on RF Superconductivity, Santa Fe, New Mexico, LANL (1999).

[39].A.Zamiri, F.Pourboghrat,H.Jiang, T.R. Bieler, F. Barlat et al, Mat. Sci.Eng A 435-436 (2006) 658-665.

[40]. O.Richmond and M.L. Devenpeck, in: US Congress on Appl Mech, ASME(1967) 1053

[41]. A.Nadai, Theory of Flow and Fracture of Solids, Vol.1,Mc-Graw-Hill, New York,1950

[42]. V.M Segal, V.I Reznikov, A.E.Drobyshevskiy and V.I Kopylov, Russian Metallurgy,(Engl Trans),1 1981 115

[43]. V.M Segal , Patent of USSR, No.575892,1977

[44]. V.M. Segal, Mater. Sci. Eng. A197 (1995) 157.

[45]. S. Ferrasse, V.M. Segal, K.T. Hartwig, R.E. Goforth, Metall.Mater. Trans. 28A (1997) 1047.

[46]. F.H. Dalla Torre, R. Lapovok, J. Sandlin, P.F. Thomson, C.H.J. Davies and E.V. Pereloma, Acta Mater. 52 (2004), 4819.

[47]. Z.C. Wang, P.B. Prangnell, Mater. Sci. Eng., A 328 (2002) 87.

[48]. J.E. Flinn, D.P. Field, G.E. Korth, T.M. Lilo, J. Macheret, Acta Mater. 49 (2001) 2065.

[49]. A. Gholinia, P.B. Prangnell and M.V. Markushev Acta Mater. 48 (2000), p. 1115.

[50]. R.E. Barber, T. Dudo, P.B. Yasskin and K.T. Hartwig, Scripta Mater. 51 (2004), p. 373.

[51]. A. Gholinia, P. Bate and P. Pragnell. Acta Mater. 50 (2002), p. 2121..

[52]. L.S. T´oth, R.A. Maisson, L. Germain, S.C. Baik, S. Suwas, Acta Mater. 52 (2004) 1885.

[53]. J.J. Beyerlein, R.A. Lebensohn and C.N. Tomé. Mater. Sci. Eng. A 345 (2003), pp. 122–138.

[54]. S. Ferrasse, V.M. Segal, S.R. Kalidindi and F. Alford, Mater. Sci. Eng. A 368 (2004), p. 28.

[55]. S. Li, I.J. Beyerlein and M.A.M. Bourke, Mater. Sci. Eng. A 394 (2005), p. 66.

[56]. S.N. Mathaudhu, R.E. Barber, K.T. Hartwig, IEEE Trans. Appl. Supercond.15 (2005) 3434–3437.

[57]. D.Bryant, M.S Thesis (2005).

[58]. D. Baars, T. R. Bieler, K. T. Hartwig, H. Jiang, C. Compton and T. L. Grimm, JOM, 59 (2007) 50-55,

[59]. H.R.Z. Sandim, H.H. Bernardi, B. Verlinden, and D. Raabe, Mater. Sci. Eng., 2007, A467, p.44–52.

[60]. Embury, J. D., Poole, W. J. & Koken, E. Scr. Metall. Mater. 27 (1992), p.1465-1470.

[61]. F.J. Humphreys, P.B. Prangnell, J.R. Bowen, A. Gholinia and C. Harris. Philos. Trans. R. Soc. A 357 (1999), pp. 1663.

[62]. W.B. Hutchinson, Met. Sci. 8 (1974), pp. 185–196.

[63]. I.L. Dillamore, J. Phys., D 7 (1974), p. 979.

[64]. L.V Raulea, L.E Govaert and F.P.T Baaijens, Geiger M. Advanced Technology of Plasticity[C], Springer, Nuremberg (1999), pp. 939–944.

[65]. Kals.R, Vollersten F, Geiger M, in: H.J.J.Kals, (Eds.), Proccedings of 4th International.Conference on Sheet Metal, vol. II, Twente, Nederlands, Enschede (1996), pp.65-75.

[66]. D.N. Lee. Scripta Metall. Mater. 32 (1995), p. 1689.

VITA

Name:	Shreyas Balachandran
Present Address:	Department of Mechanical Engineering, Texas A&M University College Station, TX-77843, Mail Stop: 3123.
Email:	shreyas-b@tamu.edu.
Education:	B.E., Mechanical Engineering, RV College of Engineering, Bangalore, 2005 M.S., Mechanical Engineering, Texas A&M University, 2008.
Future Plans:	Continuing Ph.D. studies in Mechanics and Materials